


Article

Three-Dimensional Flow Velocity Estimation of Mountain Glacier Based on SAR Interferometry and Offset-Tracking Technology: A Case of the Urumqi Glacier No.1

Jialiang Liu ¹, Jun Zhao ^{1,*}, Zhongqin Li ^{1,2}, Zhihui Yang ¹, Jianxia Yang ¹ and Guangchao Li ³

¹ College of Geography and Environmental Science, Northwest Normal University, Lanzhou 730070, China; jl37448@outlook.com (J.L.); lizq@lzb.ac.cn (Z.L.); 18419618001@163.com (Z.Y.); yangjx_nwnu@163.com (J.Y.)

² State Key Laboratory of Cryospheric Science, Tian Shan Glaciological Station, Northwest Institute of Eco-Environment and Resources, Chinese Academy of Sciences, Lanzhou 730000, China

³ College of Geoscience and Surveying Engineering, China University of Mining & Technology, Beijing 100083, China; lgc911201@163.com

* Correspondence: zhaojun@nwnu.edu.cn

Abstract: Remote sensing estimations of glacier flow velocity could provide effective methods for the long-term monitoring of glacier flow velocity. This paper calculated the velocity in the line-of-sight (LOS) direction by combining DInSAR and offset-tracking technology with ascending and descending Sentinel-1 images of the Urumqi Glacier No.1 from 2016 to 2017. Meanwhile, the velocity in the azimuthal direction was obtained by combining MAI and offset-tracking technology. Then, the eastward, northward, and upward flow velocities were retrieved using the Helmert variance component estimation method. Finally, the standard error of the mean and mean errors of surface velocity in non-glaciated areas of the Urumqi Glacier No.1 were calculated to evaluate the accuracy of the results generated by the proposed method. The results showed: (1) The ascending LOS velocity and the descending LOS velocity were 1.812 m/a and -1.558 m/a from 2016 to 2017. The ascending azimuthal and descending azimuthal velocities were 0.978 m/a and -2.542 m/a, respectively. (2) The glacier flow velocities were 2.571 m/a and 1.801 m/a, respectively, for the eastward and northward directions. In the vertical direction, the velocity was -0.554 m/a. (3) The accuracy of the results generated by the proposed method were 0.028 m/a, 0.085 m/a, and 0.063 m/a in the east, north, and vertical directions. Therefore, it is suitable to use ascending and descending Sentinel-1 images and the study method proposed in this paper to estimate the surface flow velocity of mountain glaciers.

Keywords: glacier flow velocity; Urumqi Glacier No.1; Sentinel-1; Helmert variance component estimation; SAR interferometry technology; offset-tracking technology



Citation: Liu, J.; Zhao, J.; Li, Z.; Yang, Z.; Yang, J.; Li, G. Three-Dimensional Flow Velocity Estimation of Mountain Glacier Based on SAR Interferometry and Offset-Tracking Technology: A Case of the Urumqi Glacier No.1. *Water* **2022**, *14*, 1779. <https://doi.org/10.3390/w14111779>

Academic Editor: Chang Huang

Received: 21 March 2022

Accepted: 28 May 2022

Published: 1 June 2022

Publisher's Note: MDPI stays neutral with regard to jurisdictional claims in published maps and institutional affiliations.



Copyright: © 2022 by the authors. Licensee MDPI, Basel, Switzerland. This article is an open access article distributed under the terms and conditions of the Creative Commons Attribution (CC BY) license (<https://creativecommons.org/licenses/by/4.0/>).

1. Introduction

As an essential branch of glaciology, it is well known that glacier flow velocity is one of the critical parameters for glacier dynamics and evolutionary models [1]. Different degrees of glacier ablation on a global scale have been exhibited under climate warming. The intense melting of glaciers has exacerbated the instability of glacier dynamical systems and increased the frequency of glacier disasters [2,3]. Remote sensing estimations of glacier flow velocity could provide effective methods for the long-term monitoring of glacier flow velocity. Furthermore, they contribute to climate monitoring, glacier disaster early warning, and glacier dynamics research [4–7].

The method of optical remote sensing monitoring and synthetic aperture radar (SAR) monitoring has been widely applied for glacier flow velocity estimation. Overall, the SAR differential interferometry (DInSAR), multi-aperture interferometry (MAI), and offset-tracking technology are the main SAR monitoring methods [8–10]. DInSAR and MAI technologies can generate high-quality, continuous, and smooth velocity fields without

pixel size limitations. They are also adequate for extracting low glacier velocity from several days to tens of days in a time scale. However, the decorrelation effect severely restricts the application of DInSAR and MAI technology. Long spatial and temporal baselines of SAR images or rapid changes in the scattering characteristics of the glacier surface will lead to reduced accuracy of glacier velocity estimations, failure of phase decoupling, and complete loss of calculation results [11,12]. SAR offset-tracking technology has no requirement for image coherence, which could make up for the shortcomings of DInSAR and MAI technology. However, the offset-tracking technique has a low estimated accuracy due to the influence of the matching window size and the quality of the amplitude characteristics [13,14]. The optical remote sensing monitoring method extracts the glacier flow velocity by calculating the maximum correlation coefficient of two images [15–17]. The cross-correlation method based on optical remote sensing images has the advantages of a large coverage area, more data sources, and less terrain influence. However, this method is restricted by the spatial resolution and feature-matching algorithm of the optical image, making its accuracy vulnerable to clouds and rain [18,19].

Several theories for estimating glacier velocity for different time scales have been proposed but these theories have their limitations. For instance, DInSAR and MAI techniques often suffer from the effects of temporal and spatial decoherence. The offset-tracking technique has a low computational accuracy in glacier flow velocity solving. Simultaneously, conventional SAR interferometry techniques can only monitor the glacier velocity in the LOS or azimuth directions. Few studies of glacier 3D flow velocity have investigated the problem of the different calculation accuracy of glacier azimuthal and line-of-sight flow velocities. In addition, the a priori variance of the glacier flow velocity estimates could not be obtained accurately in 3D flow velocity solving [20–23]. This paper presents a hypothesis based on the complementary advantages of offset-tracking technology and SAR interferometry technology. Three-dimensional glacier velocity with high accuracy could be obtained by applying different velocity estimation techniques in different coherent periods and different observation directions for mountain glaciers with relatively slow motion. Consequently, this study has two primary aims: (1) to propose a remote sensing estimation method of the three-dimensional velocity of glaciers based on SAR interferometry and offset-tracking technology. (2) To evaluate the method's accuracy in remote sensing estimations of mountain glacier velocity. This new velocity estimation method could overcome the decoherence limitations of the SAR interferometry technology. Meanwhile, the problem of calculation accuracy being low when the offset-tracking technology estimates glacier velocity could be solved. In addition, the problem of the difference between the calculation accuracy of the azimuthal and line-of-sight velocities of the glacier in the traditional three-dimensional velocity calculation method was improved.

Compared to X-band SAR satellites, the Sentinel-1 in the C-band penetrates snow and ice better. It can obtain higher coherence in interferometry and provide free, practical data for glacier flow velocity estimation without cloud cover and solar illumination [24]. The Urumqi Glacier No.1 is the longest observed glacier in China with the most detailed data. It is also one of the seventeen glaciers set up by the World Glacier Monitoring Service (WGMS) for global priority monitoring [25]. In the current study, the Urumqi Glacier No.1 was taken as an example. Twenty ascending Sentinel-1 images and 20 descending Sentinel-1 images of Urumqi Glacier No.1 from September 2016 to August 2017 were selected. The glacier flow velocity in the LOS and azimuth directions was estimated by combining SAR interferometry technology and offset-tracking technology. Meanwhile, the eastward velocity, northward velocity, and upward velocity of glaciers were retrieved using the Helmert variance component estimation method. Finally, the standard error of the mean and mean errors of surface velocity in non-glaciated areas of the Urumqi Glacier No.1 were calculated to evaluate the accuracy of the results generated by the proposed method. The results were verified by the root mean square error of the difference between the measured glacier velocity of all stakes during 2016–2017 and the glacier velocity retrieved by remote sensing.

2. Study Site and Materials

2.1. Study Site

The Urumqi Glacier No.1 ($43^{\circ}07' N$, $86^{\circ}49' E$) is located on the north slope of Tiange'er peak in the middle of the Tianshan Mountains and is the source of the Urumqi River Basin (Figure 1a). The glacier valley consists of the eastern and western branches (Figure 1b). Field survey data revealed that the area of the Urumqi Glacier No.1 in 2017 was 1.542 km^2 . The area of the east branch was 0.99 km^2 , which was very close to the average area of Tianshan's glaciers published in China's second glacier catalog. According to recent measurements, the average thickness is 44.5 m . The maximum thickness of the east branch is 141 m , and the maximum thickness of the west branch is 120 m [26,27]. The 2.1 km long glacier's elevation range varied from 3743 m to 4484 m . It covered the average elevation range of glaciers in the whole Tianshan area. Thus, the Urumqi Glacier No.1 has excellent regional representation in area and altitude [28].

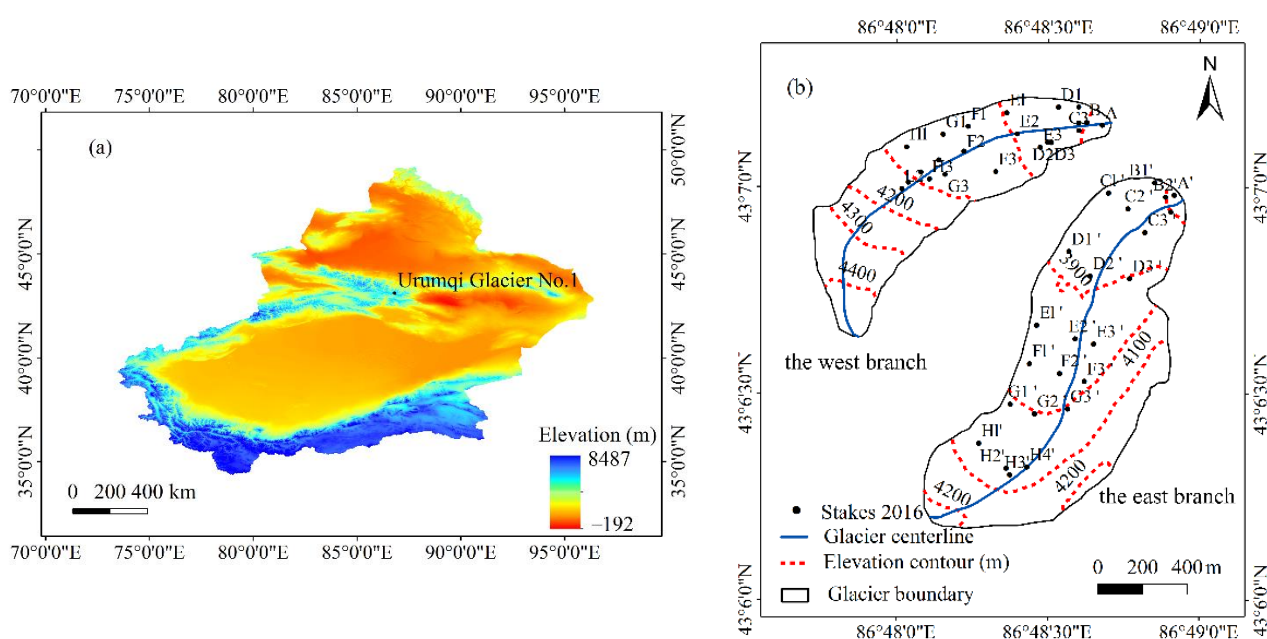


Figure 1. Study site description: (a) Location map of Urumqi Glacier No.1; (b) Sketch view of the study, including the locations of Urumqi Glacier No.1 and stakes in 2016.

2.2. Materials

The remote sensing estimation of the flow velocity of the Urumqi Glacier No.1 was mainly drawn from the following data: ascending and descending Sentinel-1 images, digital elevation model (SRTM DEM) from February 2000, glacier thickness data, and the stakes data of the Urumqi Glacier No.1. The specific data usage is shown in Table 1.

Table 1. Data used in this study.

Dataset Name	Date	Purpose of Use	Data Sources
SRTM DEM	2000-02	Generating slope map and differential interferogram after flattening	https://srtm.csi.cgiar.org (accessed on 14 June 2020)
Sentinel-1	2016-09~2017-08	Estimating glacier velocity	https://scihub.copernicus.eu/dhus/ (accessed on 3 January 2021)
Stakes velocity data	2016-09~2017-08	Verification of glacier velocity	Flow velocity experiment of Urumqi Glacier No.1
Glacier thickness data	2012	Analysis of influencing factors of glacier velocity	References: Wang et al. [27]

The flow velocity of the Urumqi Glacier No.1 from 2016 to 2017 was estimated using 20 Sentinel-1 ascending and 20 Sentinel-1 descending tracks images. The specific parameters of all Sentinel-1 interference pairs used in this study are shown in Table A1 of Appendix A. To validate the flow velocity of the Urumqi Glacier No.1, 24 stakes were placed at altitudes between 3800 and 4200 m in the east branch of the glacier, as shown in Figure 1b. These stakes were named A', B1', B2' ... I' according to their altitudes from low to high. Correspondingly, 20 stakes called A, B1, and C1 ... I were placed on the west branch of the glacier between 3850 and 4100 m. Approximately three stakes were laid on the same cross-section of glacier branches at a distance of 100 m.

3. Methodology

3.1. Two-Pass DInSAR Technology

The two-track DInSAR technology can derive the LOS direction displacement from the imaging geometry relationship and the sensor system parameters using differential interferometry and SAR images of different time phases in the same area [29,30]. In this paper, DInSAR technology was carried out using 40 Sentinel-1 images to estimate the glacier flow velocity in the LOS direction during the high-coherence period. The relationship between the deformation value Δr and its deformation phase ϕ_{def} along the LOS direction on the glacier surface is shown in Equation (1), where λ is the wavelength.

$$\phi_{def} = \frac{4\pi}{\lambda}(-\Delta r) \quad (1)$$

As an example, using an ascending master image from 11 June 2017, and a descending slave image from 23 June 2017, the concrete steps are as follows:

(1) The first step in this process was registering SAR images accurately. Five times multiview processing in azimuth directions of the images was then performed. In the follow-up phase of the process, SRTM DEM simulated the terrain phase, which was obtained from the processing, and was deducted from the terrain phase. The differential interferograms were obtained, as shown in Figure 2. It is worth noting that most interferograms have high quality and clear streak.

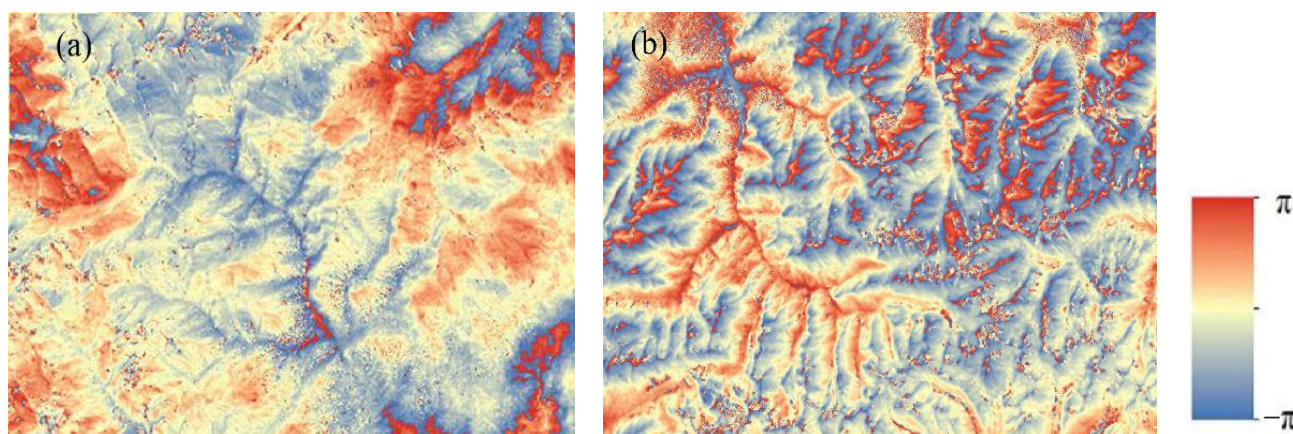


Figure 2. Interferogram after flattening. (a) the ascending Sentinel-1 pairs in 2017-06-11–2017-06-23; (b) the descending Sentinel-1 pairs in 2017-06-11–2017-06-23.

(2) The interferograms were filtered utilizing the Goldstein filter method, which used variable filters to improve the clarity of the interference fringe and reduce the noise caused by the interference image decoherence. The coherence coefficient diagrams of the master and slave images are presented in Figure 3. As shown in Figure 3, the average coherence coefficient of ascending Sentinel-1 images is 0.503, and the maximum is 0.855. The average coherence coefficient of descending Sentinel-1 images is 0.498, and the maximum value is

0.895. The coherence of two groups of coherent images is good, indicating that image pairs' similarity is good and that it is beneficial to generate interference images of good quality.

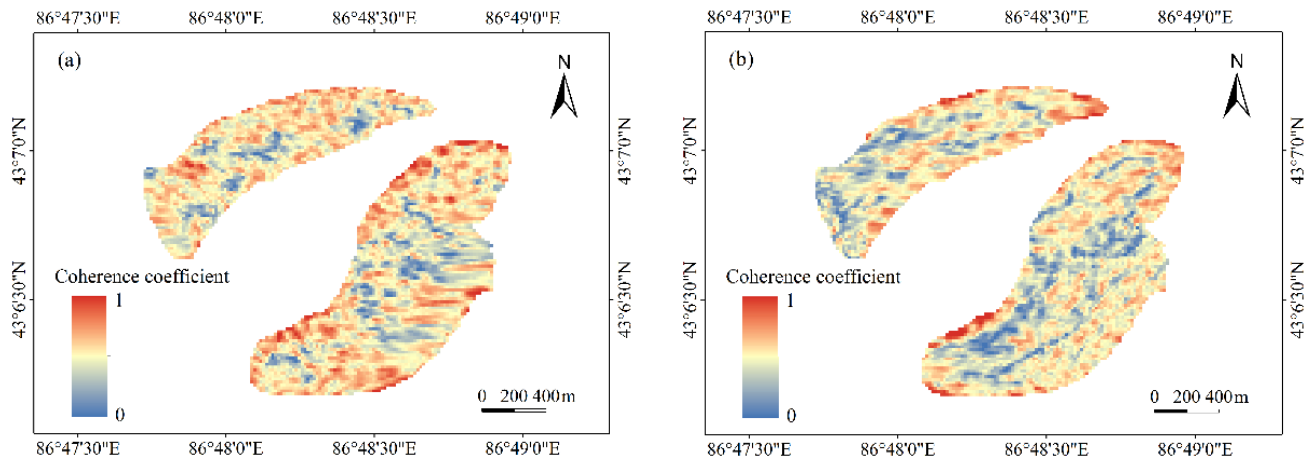


Figure 3. Coherence coefficient diagram. (a) the ascending Sentinel-1 pairs in 2017-06-11–2017-06-23; (b) the descending Sentinel-1 pairs in 2017-06-11–2017-06-23.

(3) The final stage of DInSAR technology comprised phase unwrapping, which selected the minimum cost flow method. This process also required orbit refinement and re-flattening based on control points to eliminate possible slope effects and correct satellite orbit offsets. Finally, the geographic coding was carried out. The phase information obtained by DInSAR was converted into deformation and projected into the geographic coordinate system. The flow velocity in the LOS direction of Urumqi Glacier No.1 was calculated [31,32].

3.2. Multiple Aperture Interferometry

MAI technology performed sub-beam decomposition in the azimuth direction based on the radar echoes' positive and negative Doppler frequencies. In this process, forward-looking single-look complex data with positive Doppler frequency and backward-looking single-look complex data with negative Doppler frequency were generated. Then, these data were interfered with separately to obtain the forward-looking interference phase and the backward-looking interference phase. The deformation in the azimuthal direction was acquired by the difference between the forward-looking phase and the backward-looking interference phase [33]. The MAI interference phase is shown in Equation (2):

$$\phi_{MAI} = \phi_f - \phi_b = -\frac{4\pi}{l}nx \quad (2)$$

where x denotes the deformation of glacier motion in the azimuthal direction and l is the effective antenna length. Variable n is the declination factor of the normalized radar line of sight direction. MAI technology was performed to estimate the glacier flow velocity in the azimuthal direction during high coherence time.

3.3. Offset-Tracking Technology

The current study estimated the glacier flow velocity by offset-tracking technology for the low-coherence period. Offset-tracking technology could monitor surface deformation based on SAR images, including amplitude tracking and coherence tracking. The overall offsets off can be divided into glacier motion offsets $off_{glacier}$, global offsets induced by different orbits off_{orbit} , offsets due to terrain undulation off_{topo} , ionospheric offsets $off_{ionosphere}$, and noise offsets off_{noise} [34,35]. The associated expression is as follows:

$$off = off_{glacier} + off_{orbit} + off_{topo} + off_{ionosphere} + off_{noise} \quad (3)$$

The redundant components must be removed to extract the glacier motion offsets accurately. As the influence is much slighter in middle and low latitudes, the ionosphere offset could be ignored because it is usually less than the accuracy of pixel tracking [36]. According to the information on SAR orbit parameters, the polynomial of orbit-induced offset could be fitted using the least-square method and the overall offset will be calculated [37]. The terrain undulation offset is mainly related to the perpendicular baseline [38]. The baseline length between the Sentinel-1 images used in this paper is less than 150 m. Therefore, the terrain undulation offset could be accurately compensated. Additionally, the offset caused by noise could be directly removed by median filtering [39].

3.4. Glacier Velocity Calculation Based on Helmert Variance Component Estimation

The glacier flow velocities in the LOS direction v_{LOS}^A (v_{LOS}^D) and flow velocities in the azimuthal direction v_{AZ}^A (v_{AZ}^D) can be monitored by DInSAR, MAI method, and offset tracking techniques. Here, superscript A means the ascending track and D represents the descending track. According to the relationship between line-of-sight velocity v_{LOS} and eastward velocity v_E , northward velocity v_N and upward velocity v_U , the v_{LOS} can be regarded as a combination of v_E , v_N and v_U . In order to retrieve eastward velocity v_E , northward velocity v_N , and upward velocity v_U , the methodology for solving the three-dimensional velocity on the glacier surface in Li (2018) was adopted to project and transform the line-of-sight and azimuth velocity of the glacier [40].

The relationship between v_{LOS}^A and eastward velocity v_E and northward velocity v_N for the ascending images could be expressed as:

$$v_{LOS}^A = -v_U \cdot \cos \theta^A + v_E \sin \theta^A \cdot \sin(\alpha^A - \frac{3\pi}{2}) + v_N \sin \theta^A \cdot \cos(\alpha^A - \frac{3\pi}{2}) \quad (4)$$

where, α^A and θ^A represent the azimuth and incidence angle of the ascending Sentinel-1 image.

The relationship between v_{AZ}^A and v_E and v_N can be expressed as:

$$v_{AZ}^A = -v_E \cos(\alpha^A - \frac{3\pi}{2}) + v_N \sin(\alpha^A - \frac{3\pi}{2}) \quad (5)$$

Similarly, the relationship between v_{LOS}^D and v_{AZ}^D and three-dimensional velocity of the glacier can be obtained as shown in Formulas (6) and (7).

$$v_{LOS}^D = -v_U \cdot \cos \theta^D + v_E \sin \theta^D \cdot \sin(\alpha^D - \frac{3\pi}{2}) + v_N \sin \theta^D \cdot \cos(\alpha^D - \frac{3\pi}{2}) \quad (6)$$

$$v_{AZ}^D = -v_E \cos(\alpha^D - \frac{3\pi}{2}) + v_N \sin(\alpha^D - \frac{3\pi}{2}) \quad (7)$$

where, α^D and θ^D is the azimuth and incidence angle of the descending Sentinel-1 image.

The glacier flow velocity of all images in the actual geographical coordinates is denoted by X . L represents the flow velocity of the LOS and azimuthal directions in the radar coordinate system. The following solution model is developed:

$$BX = L \quad (8)$$

where, B is the coefficient matrix of glacier flow velocity.

The azimuth velocity and the line-of-sight velocity are often contaminated by various noises in the observation process. Therefore, observation noise of glacier velocity in azimuth and line of sight direction V should be considered. The initial equation of the model is as follows:

$$BX + V = L \quad (9)$$

Let P be the weight matrix. According to the least-square criterion, the optimal estimation of the three-dimensional velocities is acquired [41] as follows:

$$\hat{X} = (B^T P B)^{-1} B P L \tag{10}$$

The key to obtaining high-precision solution results is reasonably determining the weight P of various observations. Considering that the prior variance of the observation value cannot be accurately obtained and the calculation accuracy of the glacier azimuth and LOS velocities is different, the weight is determined by the simplified Equation of Helmert variance component estimation. Its basic process is as follows:

Firstly, the glacier velocity observation values are divided into two groups according to the accuracy of the ascending LOS velocity, the descending LOS velocity, the ascending azimuth velocity, and the descending azimuth velocity. The observation matrix L_1 ($L_1 = [v_{LOS}^A \ v_{LOS}^D]^T$) of LOS glacier velocity is composed of ascending and descending LOS velocities. Azimuth glacier velocity observation matrix L_2 ($L_2 = [v_{AZ}^A \ v_{AZ}^D]^T$) is composed of ascending and descending azimuth velocity. Then, the corresponding weight matrix P ($P = [P_1 \ P_2]$) is established according to the observed values of the LOS glacier velocity and the azimuth glacier velocity.

The corresponding weight matrix P_1 and P_2 is:

$$P_1 = \begin{bmatrix} (\sigma_{LOS}^A)^2 & \\ & (\sigma_{LOS}^D)^2 \end{bmatrix} P_2 = \begin{bmatrix} (\sigma_{AZ}^A)^2 & \\ & (\sigma_{AZ}^D)^2 \end{bmatrix} \tag{11}$$

In the Equation (11), σ_{LOS}^A , σ_{AZ}^A , σ_{LOS}^D and σ_{AZ}^D are the standard deviations of v_{LOS}^A , v_{AZ}^A , v_{LOS}^D and v_{AZ}^D .

The following error equations are set out by indirect adjustment:

$$\begin{cases} V_1 = B_1 X - L_1 \\ V_2 = B_2 X - L_2 \end{cases} \tag{12}$$

where, $V_1 = [v_{LOS}^A \ v_{LOS}^D]$ and $V_2 = [v_{AZ}^A \ v_{AZ}^D]$, respectively, represent the error vectors corresponding to the two types of observations. The corresponding coefficient matrix is expressed as:

$$B_1 = \begin{bmatrix} -\cos\theta^A & \sin\theta^A \cdot \sin(\alpha^A - \frac{3\pi}{2}) & \sin\theta^A \cdot \cos(\alpha^A - \frac{3\pi}{2}) \\ -\cos\theta^D & \sin\theta^D \cdot \sin(\alpha^D - \frac{3\pi}{2}) & \sin\theta^D \cdot \cos(\alpha^D - \frac{3\pi}{2}) \end{bmatrix} \tag{13}$$

$$B_2 = \begin{bmatrix} 0 & -\cos(\alpha^A - \frac{3\pi}{2}) & \sin(\alpha^A - \frac{3\pi}{2}) \\ 0 & -\cos(\alpha^D - \frac{3\pi}{2}) & \sin(\alpha^D - \frac{3\pi}{2}) \end{bmatrix}$$

Then, the weights are determined according to the simple equation of Helmert variance component estimation. The mean square error of the unit weight of the two types of observations σ_{0i}^2 is expressed as Equation (14)

$$\sigma_{0i}^2 = \frac{V_i^T P_i V_i}{r_i} \tag{14}$$

r_i is the number of multiple observations in the class i observation. Recalculate the weight matrix using the estimated unit weight variance.

$$\bar{P}_1 = P_1 \quad \bar{P}_2 = \frac{\sigma_{01}^2}{\sigma_{02}^2} P_2 \tag{15}$$

Let $P_1 = \overline{P_1}$ $P_2 = \overline{P_2}$ be computed iteratively until $\sigma_{01}^2 \approx \sigma_{02}^2$ is estimated to obtain P . Finally, the three-dimensional velocity of the glacier surface is calculated according to Equation (10).

4. Results

This paper first used the coherence thresholds of the LOS and azimuthal directions of the Sentinel-1 images to screen the image pairs with high and low coherence of the Urumqi glacier No.1. Then, the LOS velocity in the high-coherence period was calculated by DInSAR technology and the azimuth velocity in the high-coherence period was obtained by MAI technology. Meanwhile, the glacier flow velocity in the period of low coherence between LOS and azimuth was determined using offset-tracking technology. Eventually, the Helmert variance component estimation method was used to estimate the velocity in the eastward, northward, and upward directions. The temporal and spatial distribution characteristics of the flow velocity of the Urumqi Glacier No.1 were analyzed.

4.1. The Coherence Calculation of Sentinel-1 Images

Ascending Sentinel-1 image pairs from 10 August 2017 and 22 August 2017 were taken as an example. Further, the LOS and azimuthal motion displacements of the non-glacial areas near the Urumqi Glacier No.1 were calculated using DInSAR and MAI methods under different coherence thresholds (Figure 4).

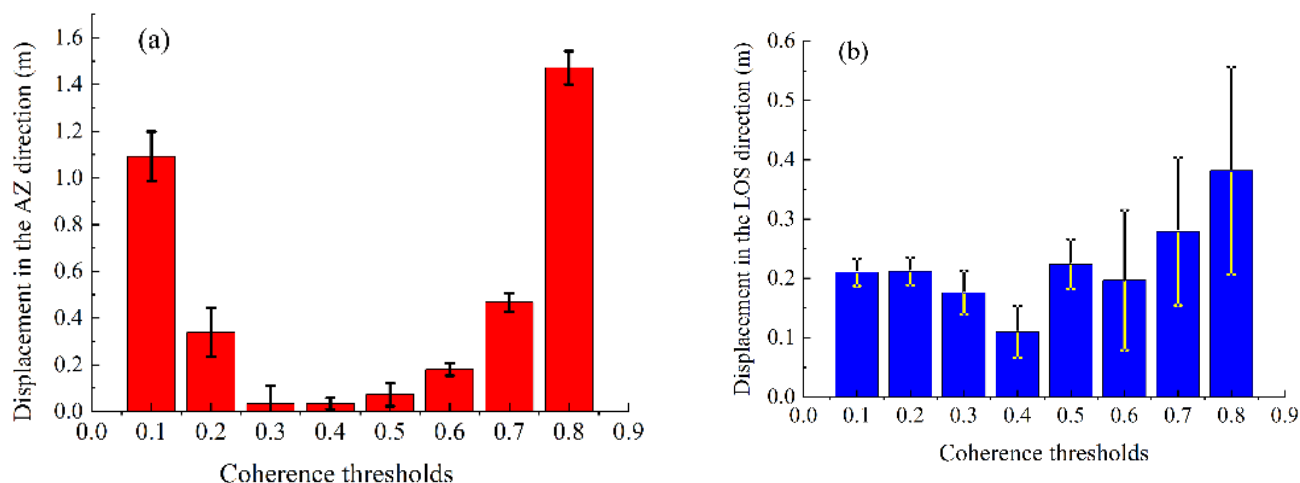


Figure 4. Displacement in the non-glacial area under different coherence thresholds. (a) Displacement in the azimuthal direction; (b) Displacement in the LOS direction.

The experiment shows that the azimuthal and LOS directions have the slightest displacement of the non-glacial zone under the circumstance that the coherence threshold is 0.4. The azimuthal and LOS motion displacements are 0.034 m and 0.109 m, respectively. Therefore, 0.4 was chosen as the coherence threshold for the azimuthal and LOS directions. The sentinel-1 pairs with a coherence higher than 0.4 were highly coherent image pairs. The DInSAR and MAI techniques were chosen to calculate the glacier flow velocity. The image pairs with a coherence lower than 0.4 were low-coherence image pairs. The flow velocity was estimated using the offset-tracking technique. The coherence diagram of each image pair of the Urumqi Glacier No.1 from 2016 to 2017 is displayed in Figures A1 and A2 in Appendix A. These coherence diagrams suggest that the coherence of most images is good. However, the images from 23 February 2017 to 31 March 2017 and 8 September 2016 to 14 October 2016 were de-coherent. Simultaneously, the coherence coefficients for all master and slave image pairs indicate that the coherence coefficients for the ascending and descending orbit images from 8 September 2016 to 14 October 2016 were 0.367 and 0.339, respectively. The coherence coefficients for the ascending and descending images

from 23 February 2017 to 31 March 2017 were 0.365 and 0.316, respectively. Their coherence coefficients were all less than the coherence threshold of 0.4.

The decoherence phenomenon in these two periods stems from the scattering characteristics of the Urumqi Glacier No.1 in the same period. April and September are the changeover periods between the summer and winter seasons in the Urumqi basin [42]. When a glacier changes from an accumulation phase to an ablation phase, the increase in temperature leads to the gradual melting of the glacier surface and the glacier interior. The rapid melting of snow and firmness on the glacier surface increases the moisture content of the ice surface, which in turn produces diffuse reflections similar to water, weakening the radiation intensity of the glacier surface's feature targets [43]. During the transition from the ablation period to the accumulation period, the temperature decreases could lead to the glacial meltwater freezing into ice. The ice surface gradually compacts with increased overlying pressure, forming hard and solid glacial ice after recrystallization and other metamorphic effects. The significant variations in the scattering characteristics of the glacier surface between the ablation and freezing periods contribute to a more severe loss of coherence [44].

4.2. Glacier Line-of-Sight and Azimuth Velocity Acquisition

The glacier velocity of the ascending and descending LOS directions was estimated by combing DInSAR and offset-tracking technology based on the ascending and descending Sentinel-1 image pairs of the Urumqi Glacier No.1 from September 2016 to August 2017, as shown in Figure 5.

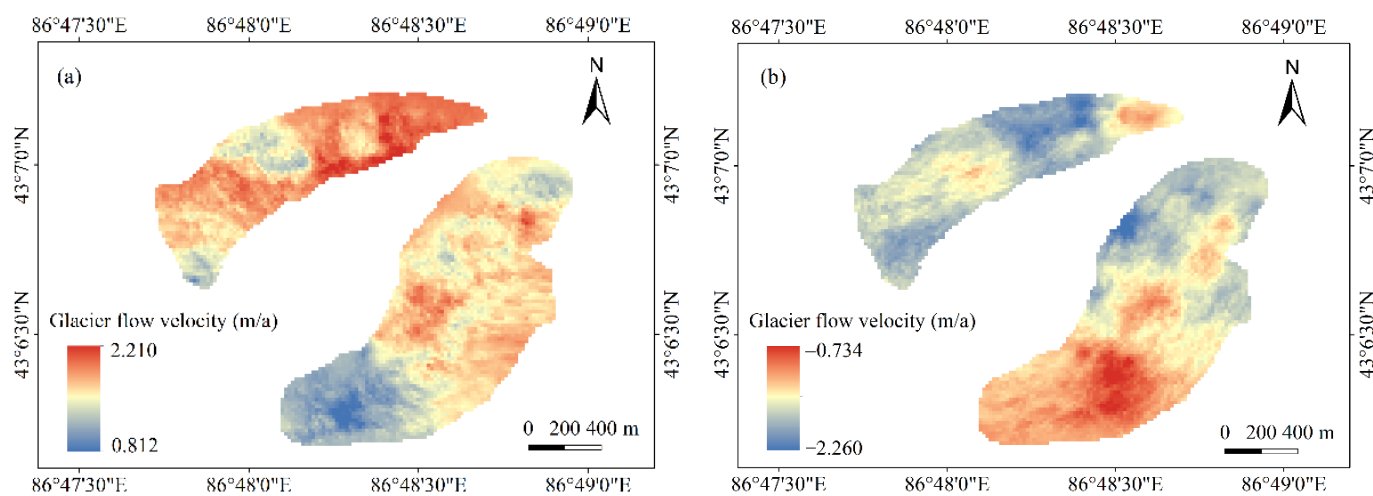


Figure 5. Glacier flow velocity of LOS direction 2016–2017: (a) LOS measurements from the ascending tracks; (b) LOS measurements from the descending tracks.

The figure shows that the LOS direction's ascending and descending glacier velocities were 1.812 m/a and -1.558 m/a from 2006 to 2007. The flow velocity of the ascending images in the west branch was 0.298 m/a higher than the glacier flow velocity of the east branch. In contrast, the velocity of the descending images in the west branch was 0.267 lower than the velocity in the east branch. Notably, the maximum LOS velocity of the ascending images was 2.210 m/a, which appeared at about 4000 m in the west branch. The maximum LOS velocity of the descending images appeared in the centerlines of the east branch with a maximum velocity of -0.734 m/a. The flow velocity distribution shows that the upper part of the glacier in the LOS direction of the ascending images moved slowly and increased as the elevation decreased. At the same time, the descending images have higher velocities in the upper region of the east branch and lower velocities at the end and edge of the glacier. Notably, the meters per year (m/a) will refer to the unit of flow velocities of the Urumqi Glacier No.1 in different directions or locations in this paper.

Based on the ascending and descending Sentinel-1 images of the Urumqi Glacier No.1 from September 2016 to August 2017, the glacier azimuth velocity was estimated by combining MAI and offset-tracking technology (Figure 6).

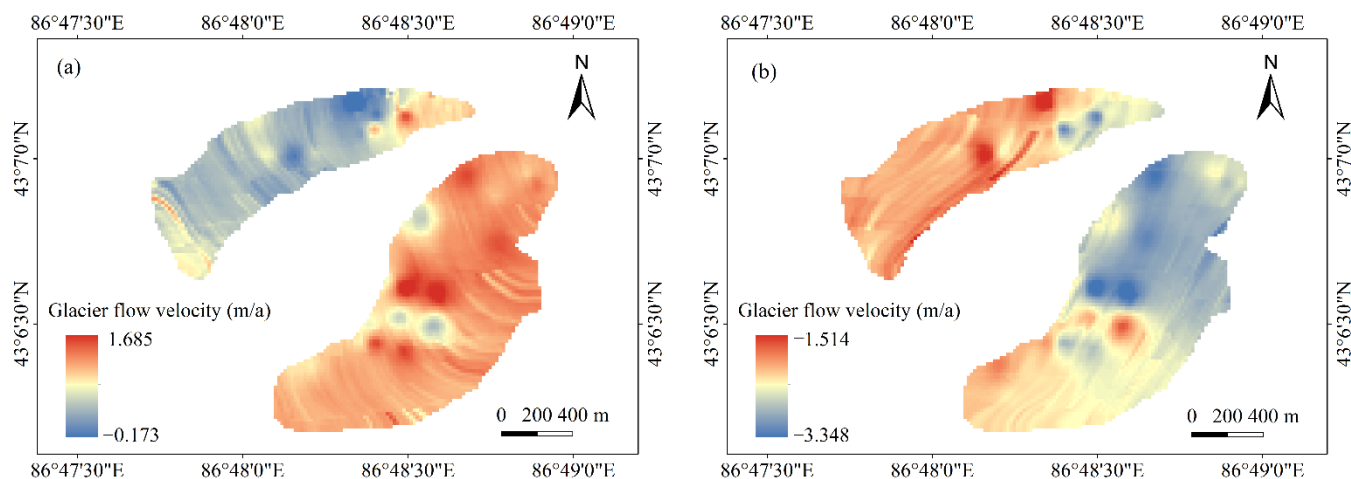


Figure 6. The glacier flow velocity of azimuthal direction 2016–2017: (a) Azimuthal measurements from the ascending tracks; (b) Azimuthal measurements from the descending tracks.

As can be seen from the figure, the glacier velocity of the azimuthal direction for the ascending images in 2016 and 2017 was 0.978 m/a. The azimuth velocity of the descending Sentinel-1 images was -2.542 m/a. According to Figure 6a, the azimuthal velocity in the accumulation area of the ascending images was lower than the velocity in the ablation area. The maximum velocity of the glacier flow was located in the area near the east branch snow line and the maximum azimuthal velocity can reach 1.685 m/a. There were some differences in azimuthal velocity between the ascending images and descending images. The velocities of the descending images were higher in the central region of the west branch and were lower in the ablation zone of the east branch. The maximum azimuthal velocity was located at about 4000 m in the west branch with a maximum velocity of -1.514 m/a. It can be seen that there were many transverse fringes because of the interference of the ionosphere in the azimuth velocity field. However, the LOS velocity field did not exist in this feature. The influence of the ionosphere could be weakened using several corrections. Nevertheless, the Sentinel azimuth estimation accuracy is usually poor, and the estimated results are unreliable even when the ionospheric effects are removed.

4.3. Distribution of the 3D Surface Flow Velocity of Urumqi Glacier No.1

Based on Helmert variance component estimation, the velocity distribution of the Urumqi Glacier No.1 in the eastward, northward, and upward directions is shown in Figure 7a–c. The three-dimensional integrated velocity was obtained by calculating the quadratic root of the square sum of the flow velocity in three directions of the Urumqi Glacier No.1, as shown in Figure 7d.

The results show that the average eastward velocity in 2016 and 2017 was 2.571 m/a, the northward flow velocity was 1.801 m/a, and the average upward flow velocity was -0.554 m/a. According to the estimated results, the eastward and upward velocities of the west branch glaciers were significantly greater than those of the east branch glaciers. This phenomenon has revealed that the larger the thickness and steeper the slope of the west branch of the Urumqi Glacier No.1, the faster the mass migration from the accumulation area to the ablation area. Moreover, the glacier area of the west branch was smaller than the glacier area of the east branch, and the glacier width was narrower than that of east branch glacier. Therefore, under the same climatic conditions, the relative shrinkage rate of the west branch glacier should be more significant than that of the east branch glacier. The northward velocity of the western glacier was slightly lower than that of the eastern

glacier, which may be due to the high rate of northward velocity decline in the west and east branches. Therefore, the velocity difference between the two branches was getting smaller and smaller.

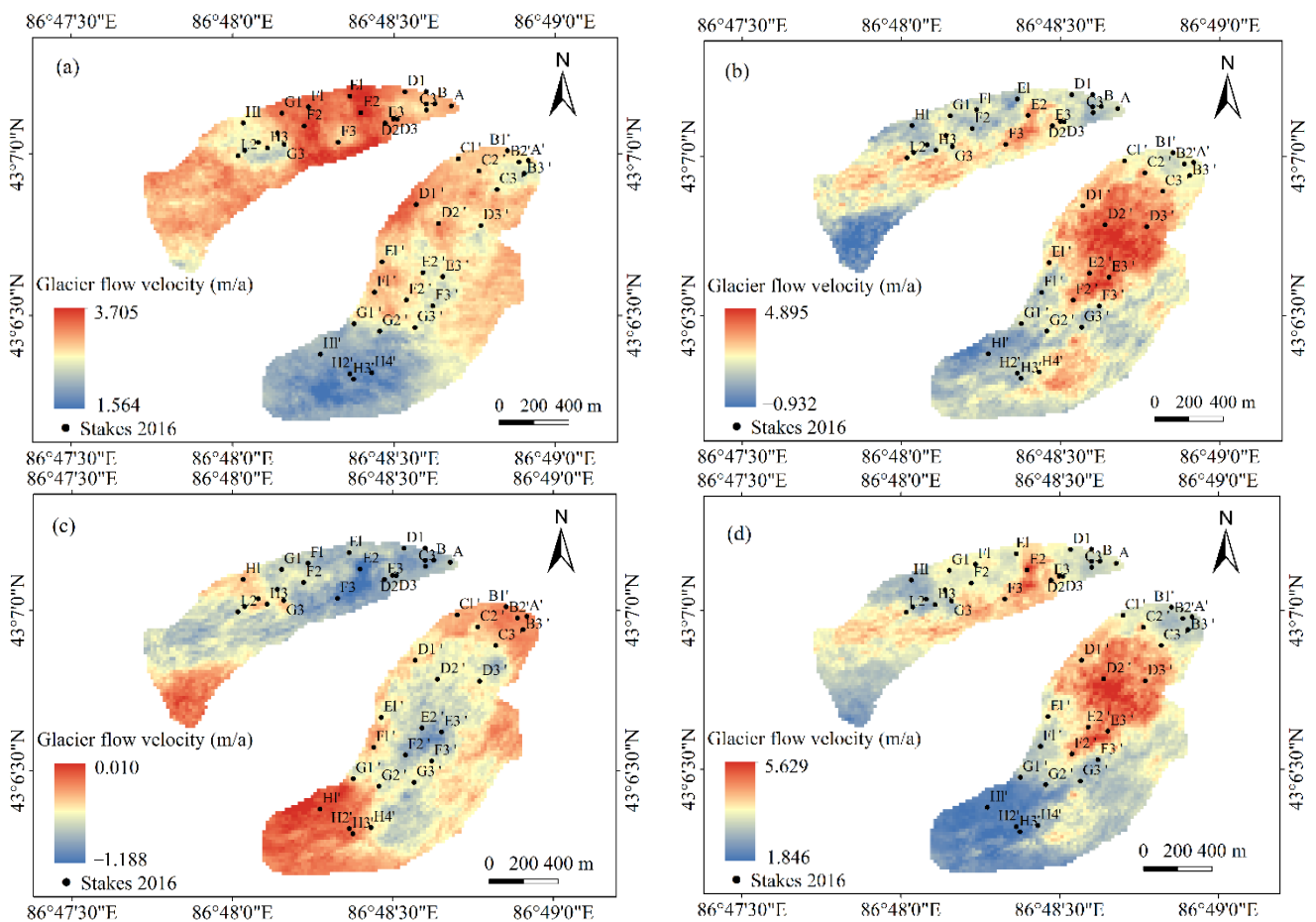


Figure 7. Spatial distribution map of glacier velocity from 2016 to 2017. (a) Velocity in the east direction; (b) Velocity in the north direction; (c) Velocity in the vertical direction (d) Three-dimensional velocity of Urumqi Glacier No.1.

In order to quantitatively analyze the annual velocity characteristics of the Urumqi Glacier No.1, the velocity results of the centerlines profile of the glacier from 2016 to 2017 were investigated. The three directions of the east and west branch were obtained, as shown in Figure 8.

According to the drawn centerlines profile (Figure 8), it can be seen that the eastward, northward, and upward flow velocities of the east branch of the Urumqi Glacier No.1 in 2016 and 2017 were 2.280 m/a, 2.327 m/a, and -0.457 m/a, respectively. On the other hand, the eastward, northward, and upward flow velocities of the west branch were 2.843 m/a, 1.834 m/a, and -0.644 m/a, respectively. As can be seen, the horizontal velocity was higher than that of the vertical direction of the centerline in the east branch. Additionally, the east and vertical flow velocities in the west branch were higher than the velocities of the same direction in the east branch. However, the north velocity was slightly lower than the east branch's. This phenomenon is likely to result from glacier thickness and slope. From the variation in the glacier flow velocity with elevation, the east, the north, and the vertical velocities of the east branch and west branch generally show a gradually increasing trend initially, followed by decreasing trend. It is probably due to glacier thickness, subglacial topography, and glacier surface morphology. The glacier flow velocity of the two branches in the horizontal direction reached a peak at the middle and lower reaches of the glacier. The vertical velocity of the glacier rose to a high point and

peaked in the middle of the glacier. At the end of the glacier, the eastward, northward, and upward velocities exhibited a fluctuation that first decreases and then increases, influenced by glacier meltwater.

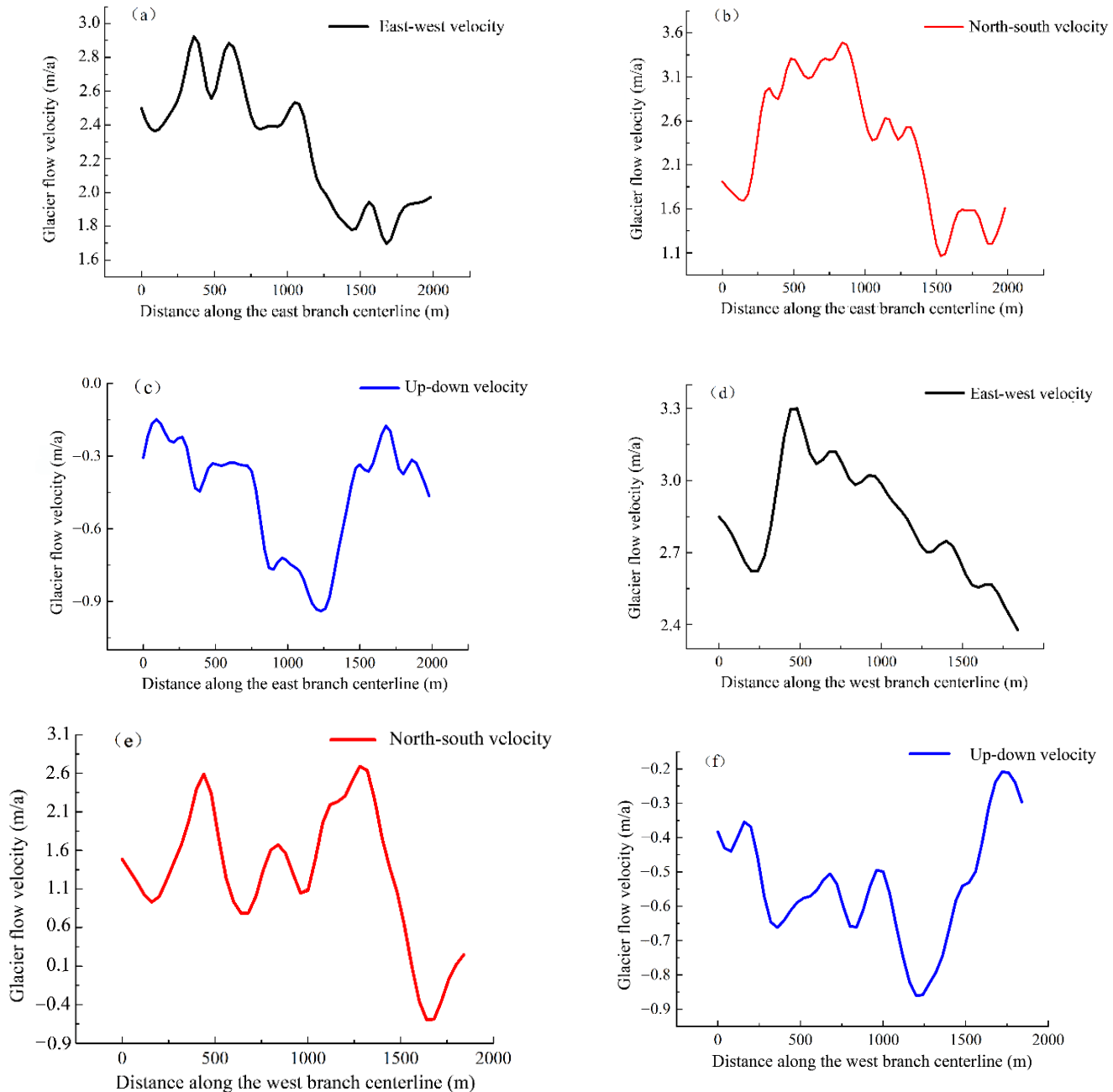


Figure 8. Glacier flow velocity along the centerlines during 2016–2017. (a–c) Show the velocity in the eastern branch. (d–f) Show the velocity in the western branch.

4.4. Accuracy Assessment and Result Verification

Based on the remote sensing estimation results of glacier velocity from 2016 to 2017, 14,784 points distributed in the non-glacial region were selected as objects for the accuracy assessment. Given the reasonable assumption that the non-glacial region is stable, the estimation method of glacier velocity was evaluated. It was calculated by the quadratic root of the sum of the mean error M_e in the non-glacial area and the standard error of the mean S_e . Figure 9 provides the accuracy evaluation results in non-glacial areas from 2016 to 2017. The figure above shows that the mean errors of surface velocity in three directions

were 0.001 m/a, 0.062 m/a, and -0.022 m/a, respectively. The mean errors of velocity were all at the centimeter level, which indicates that the noise of the velocity estimation process is slight. Glacier flow velocity error in the non-glacial region remains within ± 1.0 m/a.

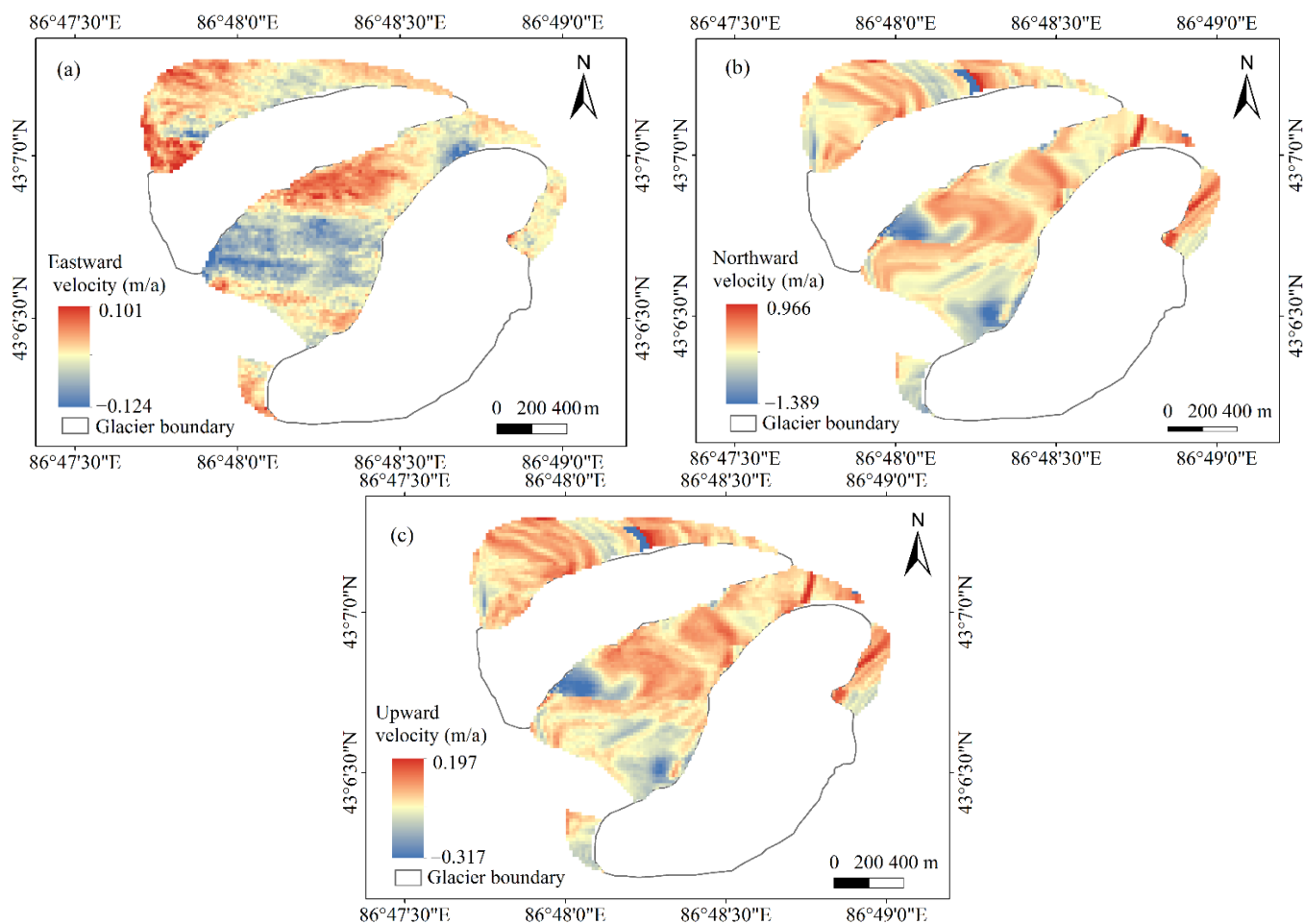


Figure 9. Glacier flow velocity error in the non-glacial region. (a) Eastward velocity error; (b) Northward velocity error; (c) Upward velocity error.

The figure above shows that the mean errors of surface velocity in three directions were 0.001 m/a, 0.062 m/a, and -0.022 m/a, respectively. The mean errors of surface velocity were all at the centimeter level, which indicates that the noise of the velocity estimation process is slight. The statistical results of non-glacial error estimation are set out in Table 2. As can be seen from the table, the accuracy of the eastward, northward, and upward glacier velocities from 2016 to 2017 were 0.028 m/a, 0.085 m/a, and 0.063 m/a, respectively. The mean error in the non-glacial area of Urumqi Glacier No.1 was 0.066 m/a. The global accuracy of the annual velocity of the Urumqi Glacier No.1 was less than 0.110 m/a, which was far lower than the average velocity of the Urumqi Glacier No.1 in all directions. It suggests that the remote sensing estimation method of glacier velocity proposed in this paper has good inversion quality, reliability, and accuracy.

Table 2. Statistical results of non-glacial errors estimation.

Velocity Direction	M_e /(m/a)	S_e /(m/a)	σ /(m/a)
Eastward velocity	0.001	0.028	0.028
Northward velocity	0.062	0.058	0.085
Upward velocity	-0.022	0.059	0.063

Note: M_e , mean error in the non-glacial area; S_e , standard error of the mean; σ , accuracy.

The estimated flow velocity of the Urumqi Glacier No.1 was compared with the glacier velocity based on the stake measurements from 2016 to 2017 to verify the results of the remote sensing estimation (Figure 10). As shown in Figure 10, the results of glacier velocity estimated by the two methods were close to each other. The average velocity difference between the two methods in the east, north, and vertical directions of the east branch from 2016 to 2017 was 0.090 m, 0.060 m, and 0.040 m, respectively. The average values of the velocity difference in the west branch were 0.108 m, 0.084 m, and -0.054 m in three directions. These results suggest that the mean error of the Urumqi Glacier No.1 velocity estimated by remote sensing was 0.131 m/a. In addition, the estimated velocity in most areas of the Urumqi Glacier No.1 was less than that measured by the stakes because the time measured by GPS RTK was longer than that estimated by the Sentinel-1 image.

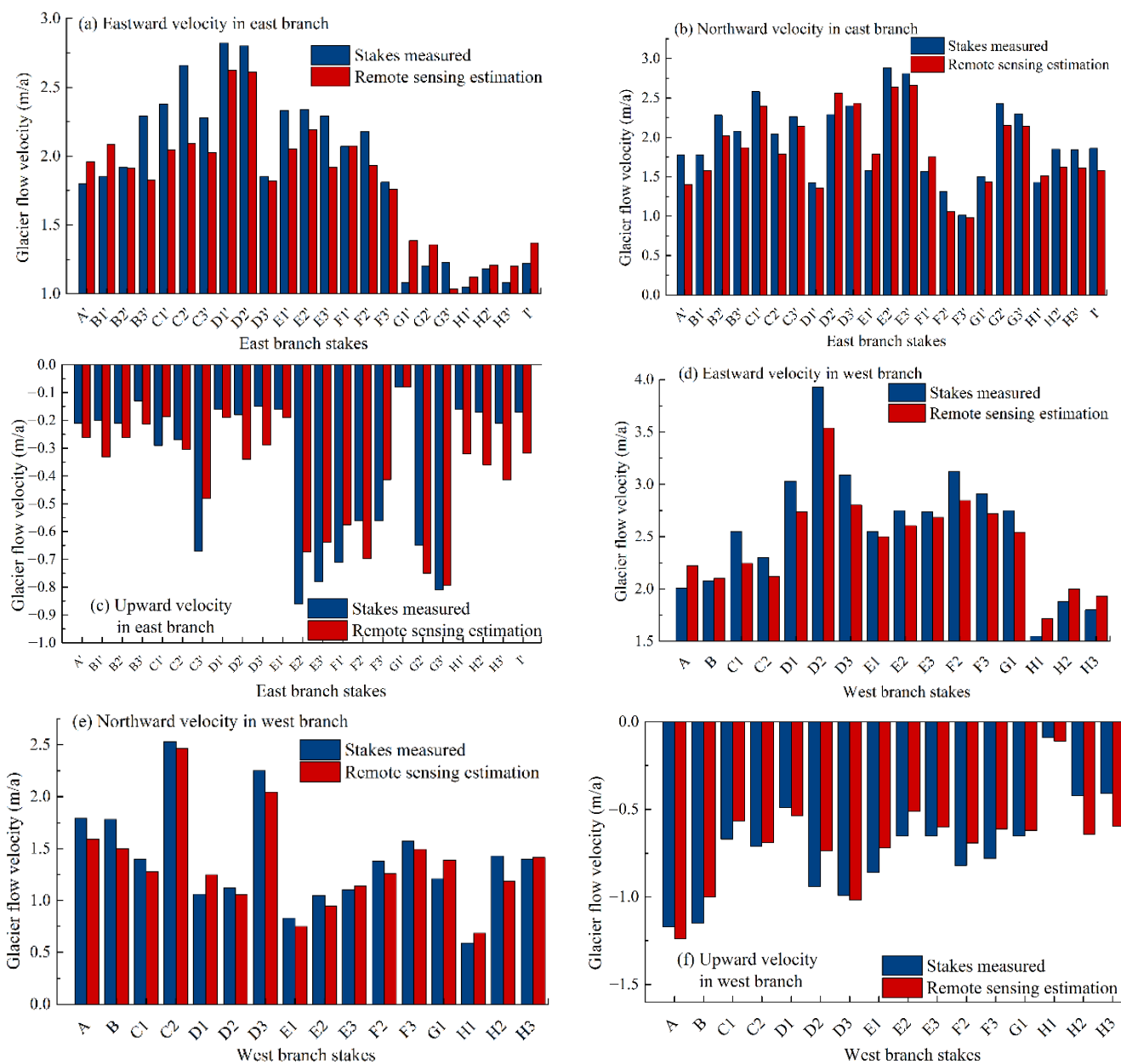


Figure 10. The comparison between the estimated glacier velocity by remote sensing and the measured glacier velocity at the stakes. (a–c) show the velocity in the east branch. (d–f) show the velocity in the west branch.

In order to assess the quality of the inversion results of glacier velocity, the results used root-mean-square error of the difference, which was between the measured velocity and the glacier flow velocity obtained from the inversion of Sentinel-1 images for all the stakes in 2016 and 2017, and were then evaluated and validated (Figure 11). The results show that the root-mean-square error of the difference between the measured velocity and inversed velocity in the east branch was 0.227 m, 0.258 m, and 0.126 m in three directions, respectively. Correspondingly, the differences between the three directions in the west branch were 0.185 m, 0.342 m, and -0.054 m, respectively. It can be inferred that the glacier flow velocity calculated based on the Helmert variance component estimation method has high accuracy. There is a significant difference between the inversion value and the measured value of glacier velocity at the individual stakes. On the one hand, the stake points could not correspond to each image element. The way that points were selected in the buffer may harm the inversion results. On the other hand, glacier surface morphology changes rapidly, giving rise to more noise and decoherence effects.

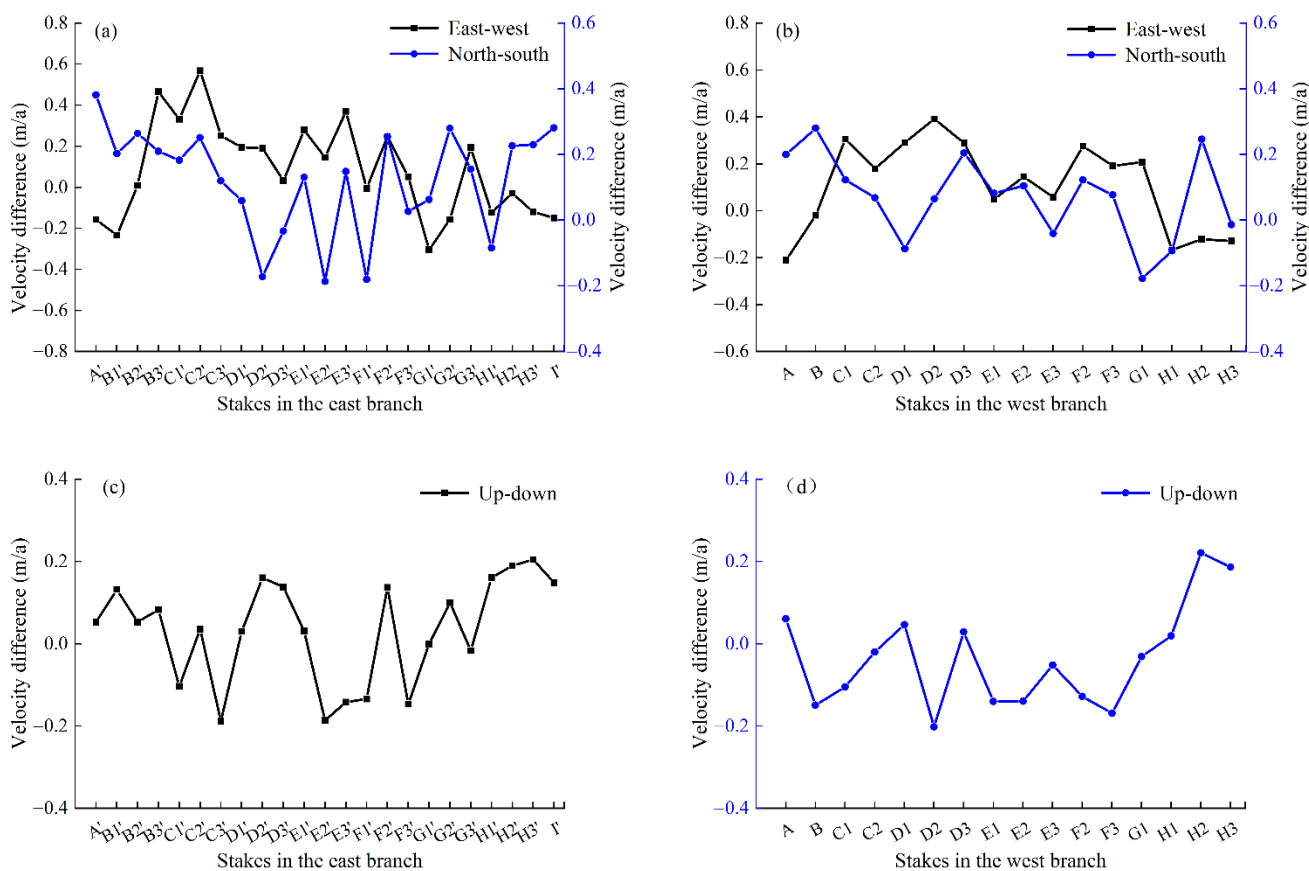


Figure 11. Difference between calculated and measured glacier flow velocity at the stakes. (a,c) show the velocity difference in the east branch. (b,d) show the velocity difference in the west branch.

5. Discussion

This study proposed a remote sensing estimation method of glacier flow velocity based on a Helmert variance component estimation. Meanwhile, the eastward, northward, and upward velocities of the Urumqi Glacier No.1 were 2.571 m/a, 1.801 m/a, and -0.554 m/a from 2016 to 2017. The accuracy of glacier flow velocity in the east, north, and vertical directions was 0.028 m/a, 0.085 m/a, and 0.063 m/a, respectively. The results show that the remote sensing estimation method of glacier flow velocity proposed in this paper could effectively provide long-term monitoring of glacier velocity.

5.1. Comparison with Other Studies

In order to facilitate a comparison with related studies in the same study area, the three-dimensional integrated flow velocity of the Urumqi Glacier No.1 was calculated to be 3.287 m/a in this paper. It is encouraging to compare the three-dimensional integrated flow velocity with that found by Wang (2021), who found that the average velocity of the Urumqi Glacier No.1 from 2017 to 2018 was 3.3 m/a using the UAV photogrammetry method [45]. Similarly, Wang (2017) monitored the motion displacement utilizing measurement stakes placed on the surface of the Urumqi Glacier No.1. Following the observation results, the studies have found that the average velocities of the Urumqi Glacier No.1 in 1980/1981, 1990/1991, 2000/2001, and 2010/2011 were 5.5 m/a, 4.6 m/a, 3.8 m/a, and 3.3 m/a, respectively. Contemporaneously, the study has revealed that the average annual velocity of the Urumqi Glacier No.1 continues to decline at 1.3% [46]. These findings suggest that the projected glacier flow velocity based on this velocity decline rate is close to the results of this paper. In addition, the motion characteristics estimated in this paper are consistent with that of Xia (2012) and Zhou (2009), which show the spatial and temporal distribution characteristics of the Urumqi Glacier No.1 as a subcontinent glacier [47,48].

To further validate the quality of the remote sensing-estimated three-dimensional velocity of the Urumqi Glacier No.1, the error analysis results with some glaciers closer to the Urumqi Glacier No.1 in time or geographic location were compared. In order to facilitate the comparison of the estimation accuracy of different algorithms, different data sources, and different glaciers, the error contribution ratio was used as a comparative index for the reliability of different glacier velocity estimation methods in this paper. The specific comparison results are shown in Table 3.

Table 3. Error comparison of different glacier velocity estimations.

Study Area	Data Source	Method	Year	Precision Evaluation Indicator	Accuracy	Error Contribution Ratio	Citation Source
Urumqi Glacier No.1	Sentinel-1	Offset tracking technology and SAR interferometry technology	2017	Mean Error	0.131 m/a	3.99%	This paper
Urumqi Glacier No.1	Sentinel-1	Offset tracking technology	2018	Mean Error	0.175 m/a	5.32%	[41]
Tuomuer-Khan Tengri Glacier	ALOS/PALSAR	Offset tracking technology	2008	Mean Error	2.02 cm/d	7.19%	[49]
South Inylchek Glacier	Landsat-8 OLI	Normalized Cross Correlation	2016	Mean Error	2.39 cm/d	6.82%	[50]
Yanong Glacier	GF-1	Normalized Cross Correlation	2017	Mean Error	7.25 m/a	5.07%	[51]
Cuolangma Glacier	Sentinel-1	PO-SBAS	2018	Mean Error	0.6 m/a	5.00%	[52]

Note: the error contribution ratio means the ratio of the mean error of the glacier velocity to the average velocity of the glacier.

Wang (2020) also obtained the glacier velocity estimation accuracy of the Urumqi Glacier No.1 in 2018 by using Offset Tracking-Small Baseline Subset (OT-SBAS) technology based on ascending Sentinel-1 images. The study found that the accuracy of the OT-SBAS estimation was 0.175 m/a [41]. Similarly, the velocity accuracy of the Urumqi Glacier No.1 in the same study period was estimated to be 0.160 m/a by combining SAR interferometry technology, offset-tracking technology, and the Helmert variance component estimation algorithm. The results indicate that the accuracy of estimating glacier velocity by combining SAR interferometry and offset-tracking technology is higher than that of using offset-tracking technology alone. For example, the Tomur Khantengri Glacier and the South Inylchek Glacier, which are located in the Tianshan Mountains of China; due to the different temporal and spatial resolutions of the algorithms and data used, the velocity estimation errors of these two glaciers are much higher than those of the Urumqi Glacier No.1. The average velocities of both non-glacier areas were much smaller than the flow velocities of the glaciers, with the error contributions of 7.19% and 6.82%, respectively [49,50]. Considering the incomplete consistency of observation periods and error factors, the glacier velocity estimation results proposed in this paper are effective and acceptable with high reliability.

5.2. Influencing Factors of Glacier Flow Velocity

A study has shown that an important factor driving glacier surface movement is glacier thickness [53,54]. The driving force for glacier flow will increase with an increasing glacier thickness, contributing to the more significant glacier flow velocity. Figure 12 analyzes the variations between the three-dimensional glacier velocity and the glacier thickness at the centerline of the glacier. This figure shows that the glacier flow velocity in the east and west branches shows a similar trend to the glacier thickness. The glacier velocity and the thickness of the glacier gradually increase as the distance from the end of the glacier increases until it reaches a maximum. From the middle of the glacier to the glacier accumulation zone, the glacier flow velocity gradually decreases with the decrease in the glacier thickness. We can conclude that a high correlation between glacier velocity and glacier thickness is evident. As mentioned in Zhou's research on the sensitivity of the velocity and thickness of the Urumqi Glacier No.1, when the Urumqi Glacier No.1 decreases by one meter in the range from 20 to 120 m, the change in glacier flow velocity ranged from 30% to 40%. Thus, the change in thickness plays a vital role in the change in glacier flow velocity [48].

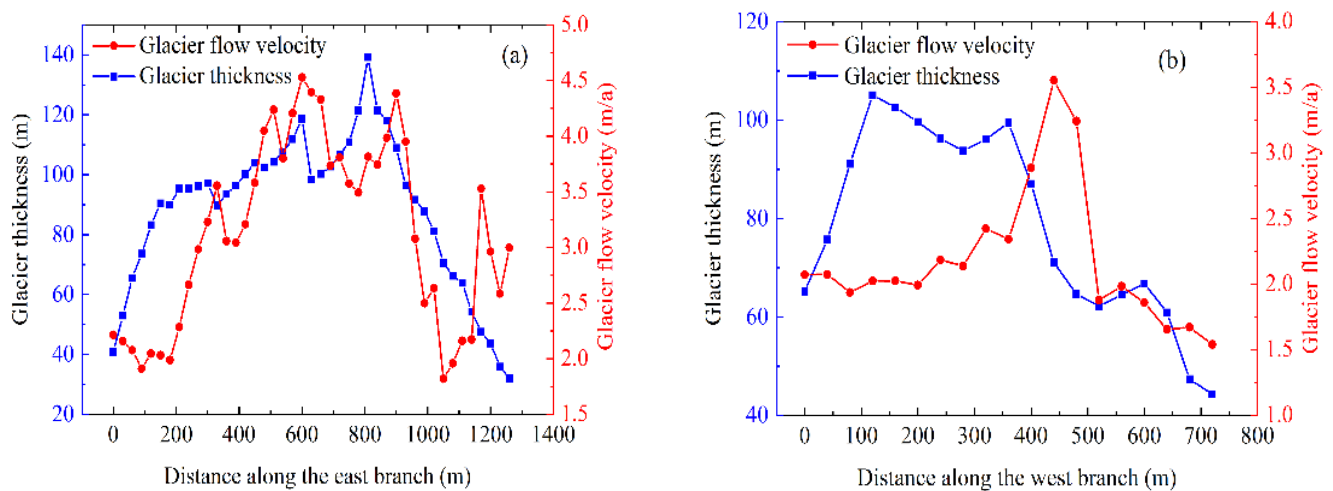


Figure 12. Glacier thickness and 3D velocity of the centerline in the east branch (a) and west branch (b).

The slope is a critical variable affecting glacier surface flow velocity [55,56]. In this paper, the surface slope of the glacier and the average velocity of the glacier were compared (Figure 13). The results illustrate that the average glacier velocity increases from 2.26 m/a to 2.681 m/a when the slope increases from 0–10° to 30–40°. However, as the slope increases further, the glacier velocity decreases. It implies that the glacier velocity is sensitive to slope changes on the glacier surface. In addition, the slope has a specific control on the velocity of the Urumqi Glacier No.1.

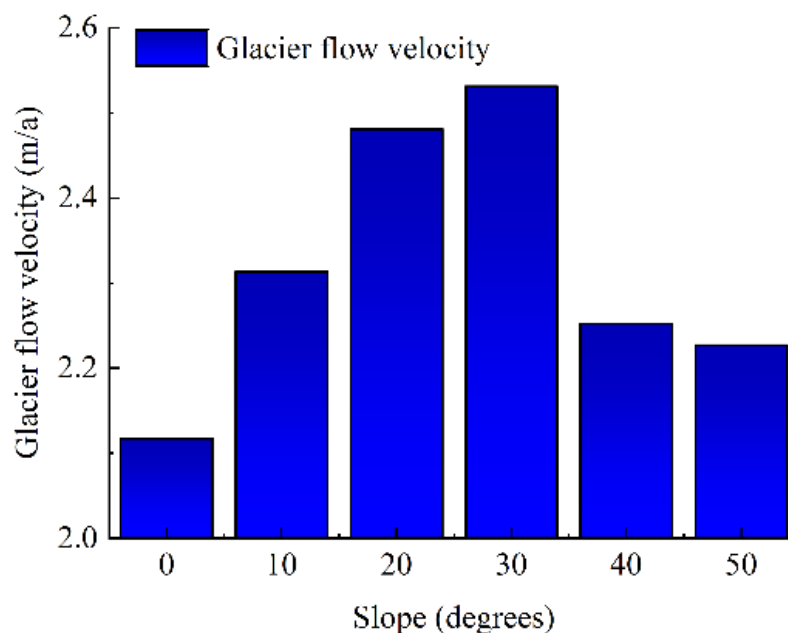


Figure 13. The variation of glacier flow velocity with slope.

Theoretically, if the glacier surface slope increases, the longitudinal slope of the glacier surface will become steeper. Further, the component of glacier gravity will become more prominent, and the glacier shear stress will increase, thus contributing to increased glacier surface motion. Conversely, the results of this study show that glacier flow velocity does not show an absolute positive correlation with the slope above a certain slope threshold. A possible explanation for this might be that the slope is too high, which is not conducive to snow accumulation. The glacier flow velocity decreases due to the thinness of the glacier. Another possible explanation for this is that the sine function of the third power of the glacier slope value increases first and then decreases in the interval $[0, \pi/2]$. At the same time, the glacier movement velocity could still reach more than 3 m/a in some glacier areas with a low slope. It further shows that the glacier surface slope will affect the glacier surface velocity, but it is not the only major factor affecting glacier velocity.

5.3. Potential Applications and Limitations of Research

The flow velocity of mountain glaciers was estimated using Sentinel-1 data and combined SAR interferometry and offset-tracking techniques in this study. However, for the high-speed moving temperate glaciers, the decoherence effect due to rapid changes in the scattering characteristics of the glacier surface may lead to this method not being applicable. Another potential problem is that Sentinel-1 images spent much computational time estimating glacier velocities due to the constraints of the computing ability of the processing platform and the vast volume of the data source. Future research will consider using Google Earth Engine (GEE) to estimate the glacier velocity based on SAR images, increasing the time series length of the study. Furthermore, several reports have shown that the estimation accuracy of glacier flow velocity could be improved by enhancing the spatial resolution of optical images [57]. Further research should be carried out to optimize the glacier flow velocity remote sensing estimation technique. The subsequent study must introduce optical images with higher spatial and temporal resolution and combine the relevant techniques, such as scale-invariant feature conversion and the acceleration robust feature, to estimate glacier velocity. Due to the limitations of the experimental conditions, the stakes that measured the data of the Urumqi Glacier No.1 were used to calculate the absolute error of the glacier velocity estimation in this paper. Future research will consider using three-dimensional laser-scanning technology to obtain glacier velocity measurement

data of a higher spatial resolution and then obtain a more accurate spatial plot of the error on the glacier surface.

The method proposed in this study has some important implications for future practice. Firstly, the research method in this paper could be used to produce large-scale glacier velocity products. It could also provide primary data for observing whole-glacier dynamics, reconstructing mountain glaciers' responses to climate warming, and analyzing glacier mass balance. With the dramatic increase in spatial and temporal resolution of remote sensing images, the method will be applied to estimate glacier flow velocity at monthly and seasonal scales and investigate long-term time series of annual glacier motion velocity. In addition, glacier equilibrium line altitude (ELA) could be detected by estimating the maximum glacier velocity. According to the glacier kinematics theory, a faster flow velocity is required to keep the glacier stable at the equilibrium line. The height at which the glacier flow velocity reaches a peak represents the ELA. The ELA could be estimated based on glacier flow velocity without mass balance data [58].

6. Conclusions

In this study, the eastward, northward, and upward flow velocities of the Urumqi Glacier No.1 from August 2016 to August 2017 were estimated using ascending and descending Sentinel-1 images, SRTM DEM, and measured data. The main conclusions are drawn as follows:

The combination of SAR interferometry technology, offset-tracking technology, and the Helmert variance component estimation algorithm could effectively estimate the three-dimensional velocity of mountain glaciers. The glacier flow velocity results of 20 m spatial resolution with 0.110 m/a estimation accuracy on a one-year time scale were obtained based on ascending and descending Sentinel-1 orbit data and the remote sensing estimation model of glacier velocity established in this paper.

The eastward and upward velocities of the west branch of the Urumqi Glacier No.1 from 2016 to 2017 were significantly higher than those of the east branch. The distribution characteristics of the surface flow velocities of the glacier's east and west branches are different in the three directions. Generally, they show a distribution trend of high in the middle and low on the sides of the same elevation zone. Meanwhile, the surface flow velocity of the Urumqi Glacier No.1 is mainly related to the thickness and slope of the glacier.

The remote sensing estimation model with combined SAR interferometry and offset-tracking techniques could provide a methodological reference for estimating mountain glacier flow velocity at different time scales. Simultaneously, it is also considered a data reference for near real-time large-scale glacier velocity mapping. In addition, this method could also estimate glacier equilibrium line altitude and glacier thickness.

Author Contributions: Conceptualization, J.Z. and J.L.; methodology, J.L.; software, J.L.; validation, J.Z., J.L. and Z.L.; formal analysis, J.L., Z.Y., J.Y. and G.L.; investigation, J.L.; resources, J.Z., Z.L. and Z.Y.; data curation, Z.L.; writing—original draft preparation, J.L.; writing—review and editing, J.L., J.Z. and Z.L.; visualization, J.L.; funding acquisition, J.Z. and Z.L. All authors have read and agreed to the published version of the manuscript.

Funding: The research reported in this manuscript is funded by the Natural Science Foundation of China (Grants No. 41761134093), Gansu Provincial Department of Education: 'Star of Innovation' Project of Excellent Graduate Students (Grants No. 2021CXZX-188).

Institutional Review Board Statement: Not applicable.

Informed Consent Statement: Not applicable.

Data Availability Statement: Not applicable.

Acknowledgments: We also sincerely thank all the editors and anonymous reviewers for their beneficial suggestions to improve the quality of this article. We would like to thank the members of

the Tien Shan Glaciological Station for supporting the field measurements. We also thank the ESA (European Space Agency) for the Sentinel-1 SAR data.

Conflicts of Interest: The authors declare no conflict of interest.

Appendix A

Table A1. Sentinel-1 image pairs used on Urumqi Glacier No.1.

Track	Master Image Acquisition Time	Slave Image Acquisition Time	Track	Master Image Acquisition Time	Slave Image Acquisition Time
Track_114-Ascending	2016-09-08	2016-10-14	Track_19-Descending	2016-09-08	2016-10-14
	2016-10-14	2016-10-26		2016-10-14	2016-11-19
	2016-10-26	2016-11-19		2016-11-19	2016-12-01
	2016-11-19	2016-12-13		2016-12-01	2016-12-13
	2016-12-13	2017-01-06		2016-12-13	2017-01-06
	2017-01-06	2017-01-30		2017-01-06	2017-01-30
	2017-01-30	2017-02-11		2017-01-30	2017-02-23
	2017-02-11	2017-02-23		2017-02-23	2017-03-31
	2017-02-23	2017-03-31		2017-03-31	2017-04-24
	2017-03-31	2017-04-24		2017-04-24	2017-05-06
	2017-04-24	2017-05-06		2017-05-06	2017-05-18
	2017-05-06	2017-05-18		2017-05-18	2017-05-30
	2017-05-18	2017-05-30		2017-05-30	2017-06-11
	2017-05-30	2017-06-11		2017-06-11	2017-06-23
	2017-06-11	2017-06-23		2017-06-23	2017-07-05
	2017-06-23	2017-07-05		2017-07-05	2017-07-17
	2017-07-05	2017-07-29		2017-07-29	2017-07-29
	2017-07-29	2017-08-10		2017-08-10	2017-08-10
	2017-08-10	2017-08-22		2017-08-22	2017-08-10

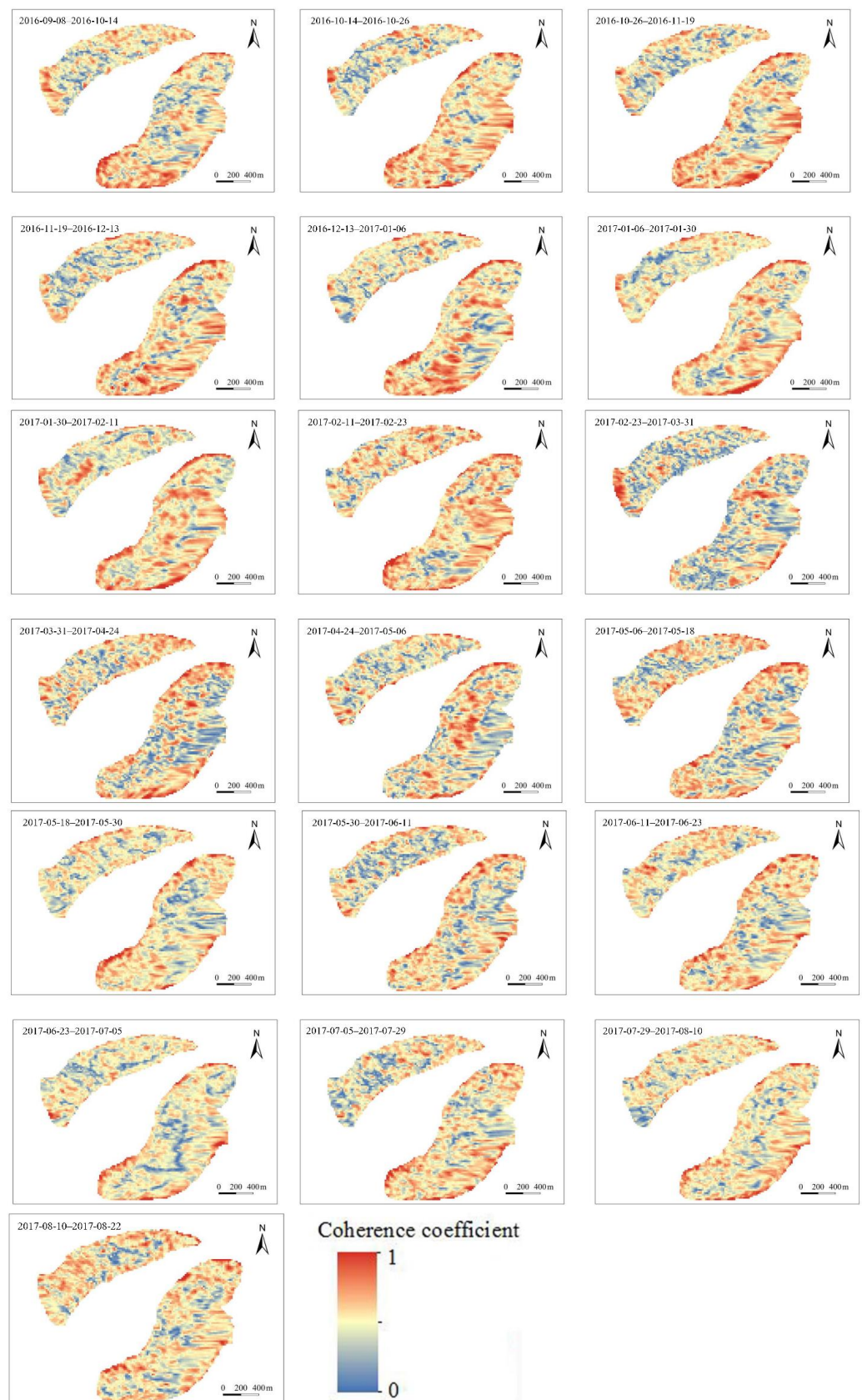


Figure A1. Coherence diagram of each ascending image pair.

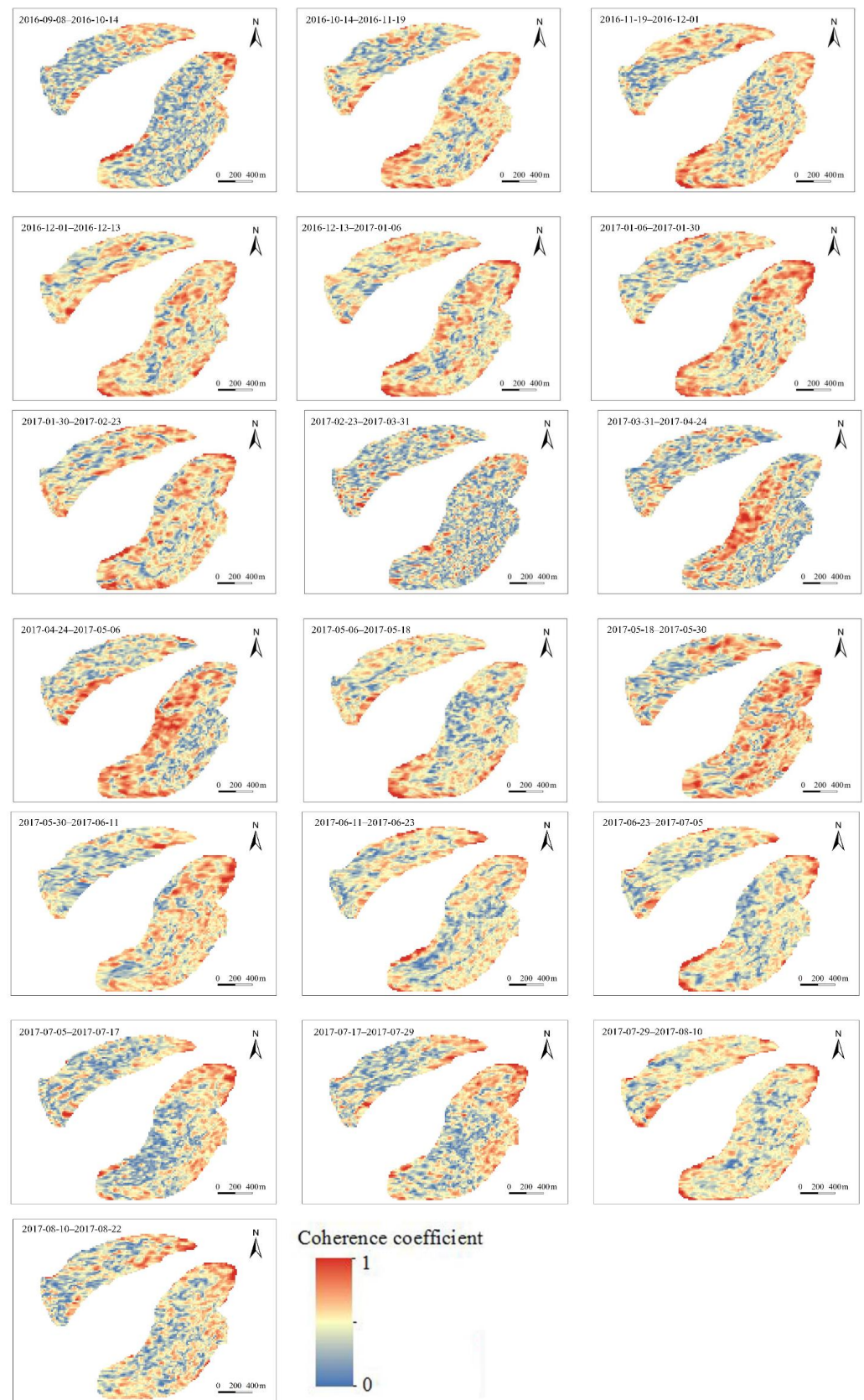


Figure A2. Coherence diagram of each descending image pair.

References

1. Faillettaz, J.; Funk, M.; Vincent, C. Avalanching glacier instabilities: Review on processes and early warning perspectives. *Rev. Geophys.* **2015**, *53*, 203–224. [[CrossRef](#)]
2. Dehecq, A.; Gourmelen, N.; Gardner, A.S.; Brun, F.; Goldberg, D.; Nienow, W.P.; Berthier, E.; Vincent, C.; Wagnon, P.; Trouvé, E. Twenty-first century glacier slowdown driven by mass loss in High Mountain Asia. *Nat. Geosci.* **2019**, *13*, 2189–2202. [[CrossRef](#)]
3. Rydt, J.D.; Reese, R.; Paolo, F.; Gudmundsson, G.H. Drivers of Pine Island Glacier speed-up between 1996 and 2016. *Cryosphere* **2021**, *15*, 113–122. [[CrossRef](#)]
4. Cai, X.R.; Li, Z.Q.; Zhang, H.; Xu, C.H. Vulnerability of glacier change in the Tianshan Mountains region of China. *J. Geogr. Sci.* **2021**, *31*, 1469–1489. [[CrossRef](#)]
5. Wu, K.P.; Liu, S.Y.; Xu, J.L.; Zhu, Y.; Liu, Q.; Jiang, Z.L.; Wei, J.F. Spatiotemporal variability of surface velocities of monsoon temperate glaciers in the Kangri Karpo Mountains, southeastern Tibetan Plateau. *J. Glaciol.* **2020**, *67*, 186–191. [[CrossRef](#)]
6. Fan, J.H.; Wang, Q.; Liu, G.; Zhang, L.; Guo, Z.C.; Tong, L.Q.; Peng, J.H.; Yuan, W.L.; Zhou, W.; Yan, J.; et al. Monitoring and Analyzing Mountain Glacier Surface Movement Using SAR Data and a Terrestrial Laser Scanner: A Case Study of the Himalayas North Slope Glacier Area. *Remote Sens.* **2019**, *11*, 625. [[CrossRef](#)]
7. Shea, J.M.; Immerzeel, W.W.; Wagnon, P.; Vincent, C.; Bajracharya, S. Modelling glacier change in the Everest region, Nepal Himalaya. *Cryosphere* **2014**, *8*, 1105–1128. [[CrossRef](#)]
8. Khanbilvardi, R.; Ganju, A.; Rajawat, A.S.; Chen, J.M.; Thakur, P.K.; Dixit, A.; Chouksey, A.; Aggarwal, S.P.; Kumar, A.S. Ice sheet features identification, glacier velocity estimation, and glacier zones classification using high-resolution optical and SAR data. *Int. Soc. Opt. Photonics* **2016**, 9877, 987719. [[CrossRef](#)]
9. Yan, S.Y.; Ruan, Z.X.; Liu, G.; Deng, K.Z.; Lv, M.Y.; Perski, Z. Deriving Ice Motion Patterns in Mountainous Regions by Integrating the Intensity-Based Pixel-Tracking and Phase-Based D-InSAR and MAI Approaches: A Case Study of the Chongce Glacier. *Remote Sens.* **2016**, *8*, 611. [[CrossRef](#)]
10. Gomez, D.; Salvador, P.; Sanz, J.; Urbazaev, M.; Casanova, J.L. Analyzing ice dynamics using Sentinel-1 data at the Solheimajokull Glacier, Iceland. *Glsci. Remote Sens.* **2020**, *57*, 813–829. [[CrossRef](#)]
11. Joughin, I.; Smith, B.E.; Abdalati, W. Glaciological advances made with interferometric synthetic aperture radar. *J. Glaciol.* **2010**, *56*, 1026–1042. [[CrossRef](#)]
12. Fallourd, R.; Harant, O.; Trouve, E.; Nicolas, J.M.; Gay, M.; Walpersdorf, A.; Mugnier, J.L.; Serafini, J.; Rosu, D.; Bombrun, L. Monitoring Temperate Glacier Displacement by Multi-Temporal TerraSAR-X Images and Continuous GPS Measurements. *IEEE J. Sel. Top. Appl. Earth Obs. Remote Sens.* **2011**, *4*, 372–386. [[CrossRef](#)]
13. Strozzi, T.; Caduff, R.; Jones, N.; Barboux, C.; Delaloye, R.; Bodin, X.; Kaab, A.; Matzler, E.; Schrott, L. Monitoring Rock Glacier Kinematics with Satellite Synthetic Aperture Radar. *Remote Sens.* **2020**, *12*, 559. [[CrossRef](#)]
14. Sun, Y.L.; Jiang, L.M.; Wang, H.S.; Liu, L.; Sun, Y.F.; Shen, Q. Detection and analysis of surface velocity over Baltoro glacier with ENVISAT ASAR data. *IEEE Int. Geosci. Remote Sens. Symp. Proc.* **2014**, *7*, 4030–4033. [[CrossRef](#)]
15. Jeong, S.; Howat, I.M.; Ahn, Y. Improved Multiple Matching Method for Observing Glacier Motion with Repeat Image Feature Tracking. *IEEE Trans. Geosci. Remote Sens.* **2017**, *55*, 2431–2441. [[CrossRef](#)]
16. Altena, B.; Scambos, T.; Fahnestock, M.; Kaab, A. Extracting recent short-term glacier velocity evolution over Southern Alaska from a large collection of Landsat data. *Cryosphere* **2019**, *13*, 795–814. [[CrossRef](#)]
17. Paul, F.; Bolch, T.; Kääb, A.; Nagler, T.; Nuth, C.; Scharrer, K.; Shepherd, A.; Strozzi, T.; Ticconi, F.; Bhamri, R.; et al. The glaciers climate change initiative: Methods for creating glacier area, elevation change and velocity products. *Remote Sens. Environ.* **2015**, *162*, 408–426. [[CrossRef](#)]
18. Eberhardt, I.D.R.; Schultz, B.; Rizzi, R.; Sanches, I.D.; Formaggio, A.R.; Atzberger, C.; Mello, M.P.; Immitzer, M.; Trabaquini, K.; Foschiera, W.; et al. Cloud Cover Assessment for Operational Crop Monitoring Systems in Tropical Areas. *Remote Sens.* **2016**, *8*, 219. [[CrossRef](#)]
19. Schaffer, N.; Copland, L.; Zdanowicz, C. Ice velocity changes on Penny Ice Cap, Baffin Island, since the 1950s. *J. Glaciol.* **2017**, *63*, 716–730. [[CrossRef](#)]
20. Kumar, V.; Venkataramana, G.; HøGda, K.A. Glacier surface velocity estimation using SAR interferometry technique applying ascending and descending passes in Himalayas. *Int. J. Appl. Earth Obs. Geoinf.* **2011**, *13*, 545–551. [[CrossRef](#)]
21. Hu, J.; Li, Z.W.; Zhu, J.J.; Ren, X.C.; Ding, X.L. Inferring three-dimensional surface displacement field by combining SAR interferometric phase and amplitude information of ascending and descending orbits. *Sci. China Earth Sci.* **2010**, *53*, 550–560. [[CrossRef](#)]
22. Wang, Q.; Fan, J.H.; Zhou, W.; Tong, L.Q.; Guo, Z.C.; Liu, G.; Yuan, W.L.; Sousa, J.J.; Perski, Z. 3D Surface velocity retrieval of mountain glacier using an offset tracking technique applied to ascending and descending SAR constellation data: A case study of the Yiga Glacier. *Int. J. Digit. Earth* **2018**, *12*, 614–624. [[CrossRef](#)]
23. Sánchez-Gómez, P.; Navarro, F.J. Glacier Surface Velocity Retrieval Using D-InSAR and Offset Tracking Techniques Applied to Ascending and Descending Passes of Sentinel-1 Data for Southern Ellesmere Ice Caps, Canadian Arctic. *Remote Sens.* **2017**, *9*, 442. [[CrossRef](#)]
24. Schwerdt, M.; Schmidt, K.; Ramon, N.T.; Klenk, P.; Yague-Martinez, N.; Prats-Iraola, P.; Zink, M.; Geudtner, D. Independent System Calibration of Sentinel-1B. *Remote Sens.* **2017**, *9*, 511. [[CrossRef](#)]

25. Wang, W.D.; Zhang, G.F.; Li, Z.Q. Study on Equilibrium Line Altitude and Its Relationship with Climate Change of Urumqi Glacier No.1 in Tianshan Mountains in Recent 52 Years. *J. Nat. Resour.* **2015**, *30*, 124–132.
26. Yue, X.Y.; Li, Z.Q.; Zhao, J.; Fan, J.; Takeuchi, N.; Wang, L. Variation in Albedo and Its Relationship with Surface Dust at Urumqi Glacier No. 1 in Tien Shan, China. *Front. Earth Sci.* **2020**, *8*, 110. [[CrossRef](#)]
27. Wang, P.Y.; Li, Z.Q.; Li, H.L.; Yao, H.B.; Xu, C.H.; Zhou, P.; Jin, S.; Wang, W.B. Analyses of recent observations of Urumqi Glacier No. 1, Chinese Tianshan Mountains. *Environ. Earth Sci.* **2016**, *75*, 720. [[CrossRef](#)]
28. Farinotti, D.; Longueuevigne, L.; Moholdt, G.; Duethmann, D.; Molg, T.; Bolch, T.; Vorogushyn, S.; Guntner, A. Substantial glacier mass loss in the Tien Shan over the past 50 year. *Nat. Geosci.* **2015**, *8*, 716–722. [[CrossRef](#)]
29. Tao, Q.X.; Gao, T.F.; Liu, G.L.; Wang, Z.W. Effect of external digital elevation model on monitoring of mine subsidence by two-pass differential interferometric synthetic aperture rada. *J. Appl. Remote Sens.* **2017**, *11*, 026037. [[CrossRef](#)]
30. Samsonov, S. Three-dimensional deformation time series of glacier motion from multiple-aperture DlnSAR observation. *J. Geod.* **2019**, *93*, 2651–2660. [[CrossRef](#)]
31. Khwaja, A.S.; Cetin, M. Improved DlnSAR time-series reconstruction in the presence of phase unwrapping errors using Huber-norm. *IET Radar. Sonar Navig.* **2019**, *13*, 1063–1073. [[CrossRef](#)]
32. Hu, J.; Li, Z.W.; Li, J.; Zhang, L.; Ding, X.L.; Zhu, J.J.; Sun, Q. Toward Complete Three-Dimensional Movements for Alpine Glacier in Qinghai-Tibetan Plateau by Integrating D-InSAR, MAI and Offset-Tracking Measurements. *Acta Geol. Sin. Engl. Ed.* **2013**, *87*, 29.
33. Jung, H.S.; Won, J.S.; Kim, S.W. An Improvement of the Performance of Multiple-Aperture SAR Interferometry (MAI). *IEEE Trans. Geosci. Remote Sens.* **2009**, *47*, 2859–2869. [[CrossRef](#)]
34. Yasuda, T.; Furuya, M. Dynamics of surge-type glaciers in West Kunlun Shan, Northwestern Tibet. *J. Geophys. Res. Earth Surf.* **2016**, *120*, 2393–2405. [[CrossRef](#)]
35. Neelmeijer, J.; Motagh, M.; Wetzel, H.U. Estimating Spatial and Temporal Variability in Surface Kinematics of the Inylchek Glacier, Central Asia, using TerraSAR-X Data. *Remote Sens.* **2014**, *6*, 9239–9259. [[CrossRef](#)]
36. Chae, S.H.; Lee, W.J.; Jung, H.S.; Zhang, L. Ionospheric Correction of L-Band SAR Offset Measurements for the Precise Observation of Glacier Velocity Variations on Novaya Zemlya. *IEEE J. Sel. Top. Appl. Earth Obs. Remote Sens.* **2017**, *10*, 3591–3603. [[CrossRef](#)]
37. Yan, S.Y.; Liu, G.; Wang, Y.J.; Perski, Z.; Ruan, Z.X. Glacier surface motion pattern in the Eastern part of West Kunlun Shan estimation using pixel-tracking with PALSAR imagery. *Environ. Earth Sci.* **2015**, *74*, 1871–1881. [[CrossRef](#)]
38. Yan, S.Y.; Zheng, Y.T.; Li, Y.; Lang, F.K.; Ruan, Z.X. A spatio-temporal variation analysis of Fedchenko and Grumm-Grzhimaylo glacier motion pattern with an efficient pixel-tracking method on spaceborne SAR imagery. *Environ. Earth Sci.* **2019**, *78*, 599. [[CrossRef](#)]
39. Yan, S.Y.; Liu, G.; Wang, Y.J.; Ruan, Z.X. Accurate Determination of Glacier Surface Velocity Fields with a DEM-Assisted Pixel-Tracking Technique from SAR Imagery. *Remote Sens.* **2015**, *7*, 10898–10916. [[CrossRef](#)]
40. Li, J.; Li, Z.W.; Wu, L.X.; Xu, B.; Hu, J.; Zhou, Y.S.; Miao, Z.L. Deriving a time series of 3D glacier motion to investigate interactions of a large mountain glacial system with its glacial lake: Use of Synthetic Aperture Radar Pixel Offset-Small Baseline Subset technique. *J. Hydrol.* **2018**, *559*, 596–608. [[CrossRef](#)]
41. Wang, Y.Q.; Zhao, J.; Li, Z.Q.; Zhang, M.J.; Wang, Y.C.; Liu, J.L.; Yang, J.X.; Yang, Z.H. Retrieving and Verifying Three-Dimensional Surface Motion Displacement of Mountain Glacier from Sentinel-1 Imagery Using Optimized Method. *Water* **2021**, *13*, 1793. [[CrossRef](#)]
42. Jiao, K.Q.; Jing, Z.F.; Han, T.D.; Yang, H.A.; Ye, B.S.; Li, Z.Q. Variation of the Glacier No.1 at the Headwaters of the Urumqi River in the Tianshan Mountains during the Past 42Years and Its Trend Prediction. *J. Glaciol. Geocryol.* **2004**, *3*, 253–260.
43. Sansosti, E.; Berardino, P.; Bonano, M.; Calo, F.; Castaldo, F.; Casu, F.; Manunta, M.; Manz, M.; Pepe, A.; Pepe, S.; et al. InSAR-based Glacier Velocity Mapping in the Parlung Zangbo River Basin, Tibetan Plateau, China. *Korean J. Remote Sens.* **2019**, *35*, 15–28. [[CrossRef](#)]
44. Goldstein, R.M.; Engelhardt, H.; Kamb, B.; Frolich, R.M. Satellite Radar Interferometry for Monitoring Ice Sheet Motion: Application to an Antarctic Ice Stream. *Science* **2018**, *262*, 1525–1530. [[CrossRef](#)] [[PubMed](#)]
45. Wang, P.Y.; Li, H.L.; Li, Z.Q.; Liu, Y.S.; Xu, C.H.; Mu, J.X.; Zhang, H. Seasonal Surface Change of Urumqi Glacier No. 1, Eastern Tien Shan, China, Revealed by Repeated High-Resolution UAV Photogrammetry. *Remote Sens.* **2021**, *13*, 3398. [[CrossRef](#)]
46. Wang, P.Y.; Li, Z.Q.; Zhou, P.; Li, H.L.; Yu, G.B.; Xu, C.H.; Wang, L. Long-term change in ice velocity of Urumqi Glacier No. 1, Tian Shan, China. *Cold Reg. Sci. Technol.* **2018**, *145*, 177–184. [[CrossRef](#)]
47. Xia, M.Y.; Li, Z.Q.; Wang, W.B. Research on characteristics variation of east and west branches of Glacier No.1 at the headwaters of Urumqi River. *J. Arid. Land Resour. Environ.* **2012**, *26*, 40–44.
48. Zhou, Z.M.; Li, Z.Q.; Li, H.L.; Jing, Z.F. The Flow Velocity Features and Dynamic Simulation of the Glacier No.1 at the Headwaters of Urumqi River, Tianshan Mountains. *J. Glaciol. Geocryol.* **2009**, *31*, 55–61.
49. Li, J.; Li, Z.W.; Zhu, J.J.; Ding, X.L.; Wang, C.C.; Chen, J.L. Deriving surface motion of mountain glaciers in the Tuomuer-Khan Tengri Mountain Ranges from PALSAR images. *Glob. Planet. Chang.* **2013**, *101*, 61–71. [[CrossRef](#)]
50. Li, Y.; Yan, S.Y.; Li, Z.G.; Zhou, H.Y.; Zheng, Y.T.; Liu, Q.Q. The flow state of South Inylchek Glacier in the Tianshan Mountains in 2016: Extraction and analysis based on Landsat-8 OLI image. *J. Glaciol. Geocryol.* **2017**, *39*, 1281–1288.
51. Zhou, J.M.; Zhang, X.; Liu, Z.P.; Li, Z. Extraction and analysis of mountain glacier movement from GF-1 satellite data. *Natl. Remote Sens. Bull.* **2021**, *25*, 530–538.

52. Yang, L.Y.; Zhao, C.Y.; Lu, Z.; Yang, C.S.; Zhang, Q. Three-dimensional time series movement of the cuolangma glaciers, southern tibet with sentinel-1 imagery. *Remote Sens.* **2020**, *12*, 3466. [[CrossRef](#)]
53. Cuffey, K.M.; Paterson, W.S.B. *The Physics of Glaciers*, 4th ed.; Elsevier: Amsterdam, The Netherlands, 2010; pp. 301–315.
54. Pandey, P.; Banerjee, D.; Ray, P. A satellite-based comprehensive observation of glaciological characteristics of Shunkalpa (Ralam) Glacier, Central Himalaya, India. *J. Earth Syst. Sci.* **2021**, *130*, 139. [[CrossRef](#)]
55. Wu, Z.; Liu, S.Y.; He, X.B. Numerical simulation of the flow velocity and temperature of the Dongkemadi Glacier. *Environ. Earth Sci.* **2016**, *75*, 394. [[CrossRef](#)]
56. Gantayat, P.; Kulkarni, A.V.; Srinivasan, J. Estimation of ice thickness using surface velocities and slope: Case study at Gangotri Glacier, India. *J. Glaciol.* **2014**, *60*, 277–282. [[CrossRef](#)]
57. Scherler, D.; Strecker, M.R. Large surface velocity fluctuations of Biafo Glacier, central Karakoram, at high spatial and temporal resolution from optical satellite images. *J. Glaciol.* **2012**, *58*, 569–580. [[CrossRef](#)]
58. Sakai, A.; Nuimura, T.; Fujita, K.; Takenaka, S.; Nagai, H.; Lamsal, D. Climate regime of Asian glaciers revealed by GAMDAM glacier inventory. *Cryosphere* **2015**, *9*, 865–880. [[CrossRef](#)]